Journal of Polymers and the Environment (2025) 33:2515–2536
https://doi.org/10.1007/s10924-025-03543-2

ORIGINAL PAPER

Fabrication and in Vivo Evaluation of Hybrid Squalene-Loaded Nanofiber Scaffolds Based on Poly(ε-Caprolactone)/Polyvinyl Alcohol/ Chitosan for Wound Healing Applications

Fariba Noori[1] · Azam Bozorgi[2,3] · Ahmad Reza Farmani[1] · Ali Abbasi[4] · Jafar Ai[5] · Alireza Tavassoli[6] · Abdolmajid Ghasemian[7] · Hassan Morovvati[8] · Hiva Alipanah[4] · Mohammad Reza Ataollahi[9] · Lida Ebrahimi[1] · Seyed Amin Kouhpayeh[10] · Arash Goodarzi[1]

Accepted: 21 February 2025 / Published online: 6 March 2025

Abstract

Chronic wounds significantly burden global healthcare systems, necessitating innovative solutions. Hybrid electrospun nanofibers are promising for enhancing wound healing and controlled drug delivery. This study focused on developing and characterizing hybrid nanofibrous scaffolds made from polycaprolactone (PCL), polyvinyl alcohol (PVA), and chitosan (Cs), infused with squalene (SQ) to improve healing in a rat model of full-thickness wounds. The scaffolds were created using coaxial electrospinning, with PCL as the shell and a PVA/Cs mixture as the SQ-loaded core. Characterization involved Fourier-transform infrared spectroscopy (FTIR), Scanning Electron Microscope (SEM), mechanical properties, contact angle measurements, swelling, degradation, drug release, cell attachments and cytotoxicity assays. After

✉ Seyed Amin Kouhpayeh
kouhpayeha@gmail.com

✉ Arash Goodarzi
dvm.goodarzi86@yahoo.com

Fariba Noori
Faribanoori99@gmail.com

Azam Bozorgi
abozorgi1991@gmail.com

Ahmad Reza Farmani
ahmadrezafarmani66@gmail.com

Ali Abbasi
abbasiali936@gmail.com

Jafar Ai
jafar_ay2000@yahoo.com

Alireza Tavassoli
tavaspath790@yahoo.com

Abdolmajid Ghasemian
majidghasemian86@gmail.com

Hassan Morovvati
hmorovvati@ut.ac.ir

Hiva Alipanah
alipanah.hiwa@yahoo.com

Mohammad Reza Ataollahi
ataollahimr@gmail.com

Lida Ebrahimi
lida_ebrahimi56@yahoo.com

[1] Department of Tissue Engineering, School of Advanced Technologies in Medicine, Fasa University of Medical Sciences, Fasa, Iran

[2] Department of Tissue Engineering, School of Medicine, Kermanshah University of Medical Sciences, Kermanshah, Iran

[3] -Fertility and Infertility Research Center, Health Technology Institute, Kermanshah University of Medical Sciences, Kermanshah, Iran

[4] Department of Physiology, Fasa University of Medical Sciences, Fasa, Iran

[5] Department of Tissue Engineering, School of Advanced Technologies in Medicine, Tehran University of Medical Sciences, Tehran, Iran

[6] Department of Pathology, School of Medicine, Fasa University of Medical Sciences, Fasa, Iran

[7] Noncommunicable Diseases Research Center, Fasa University of Medical Sciences, Fasa, Iran

[8] Department of Comparative Histology, Faculty of Veterinary Medicine, University of Tehran, Tehran, Iran

[9] Department of Immunology, School of Medicine, Fasa University of Medical Sciences, Fasa, Iran

[10] Department of Pharmacology, School of Medicine, Fasa University of Medical Sciences, Fasa, Iran

implantation in a rat model for 14 days, histopathological assessments evaluated inflammation, re-epithelialization, and collagen deposition. The hybrid nanofibers maintained consistent morphology with smooth surfaces and no bead formation. Diameters were 219 ± 33.4 nm for the neat scaffold and 227 ± 59.7 nm, 167.3 ± 35.9 nm, and 126.7 ± 39.75 nm for SQ2%, SQ3%, and SQ4%, respectively. SQ-loaded scaffolds exhibited reduced swelling ratio, hydrophilicity, and degradation rate, alongside improved tensile strength (194% increase in SQ4% vs. control), sustained SQ release (40% over 14 days for SQ3%), as well as considerable reducing in wound sizes (90% reduction in SQ2%). The PCL-PVA/Cs/SQ2% formulation notably reduced inflammation while promoting re-epithelialization and collagen deposition. The PCL-PVA/Cs/SQ nanofiber scaffolds demonstrated superior properties that effectively modulated inflammation and promoted wound healing. They represent a promising strategy for enhancing wound repair.

Graphical Abstract

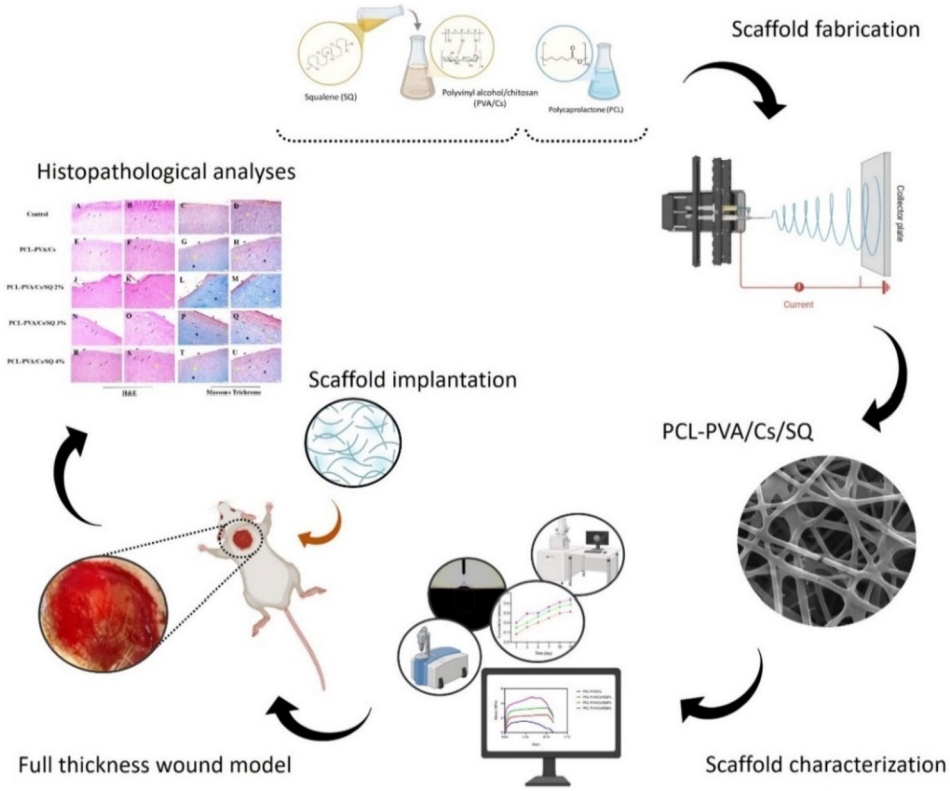

Keywords Wound Healing · Tissue Engineering · Hybrid Nanofibers · Drug Delivery · Squalene

Introduction

Skin is the largest organ of the human body, and it has critical roles in protecting against injuries and pathogens, preventing body dehydration, initiating vitamin D synthesis, regulating body temperature, and acting as a sensory organ receiving touch, pain, and temperature changes [1]. Skin injuries following traumas (cuts, lacerations, and punctures), or burns by physical and chemical reagents, and some infections could cause health issues, thus requiring local and systemic treatments to promote wound healing and prevent scar formation [2]. Wound healing involves a series of intricate processes that can be categorized into four overlapping yet distinct phases: tissue homeostasis, inflammation, proliferation, and remodeling. The progression through these phases is tightly regulated by the interactions of various cell types, as well as by the influence of growth factors, cytokines, and chemokines [3].

The lack of coordination among the phases of wound healing can result in incomplete repair, leading to chronic wounds or scarring, both of which are highly undesirable and impose significant costs on patients and healthcare systems [4, 5]. Furthermore, the risk of infection, particularly hospital-acquired infections, along with the development of

antibiotic resistance, exacerbates these challenges [6]. Consequently, it is essential to explore innovative strategies for accelerating wound healing.

Skin tissue engineering focuses on developing biomaterial-based wound dressings and skin substitutes with strong antibacterial and anti-inflammatory properties to fasten wound healing and tissue repair and avoiding impaire wound healing [7]. Wound dressings should create a mechanically stable physical defensive barrier against environmental factors to prevent wound infection and dehydration while enabling cellular attachment and migration at the injury site [8]. Among various types of wound dressings, electrospun nanofibers attract much attention because they can be obtained using simple and cost-effective methods and being biomimetics [9]. Electrospun nanofibers own appropriate properties like high surface area, microporosity, and potential to load various drugs and bioactive molecules, encouraging cell proliferation and wound healing [10].

Moreover, electrospun nanofibers have gained significant attention as advanced materials for wound dressings due to their unique properties, including high porosity, large surface area-to-volume ratio, and structural similarity to the extracellular matrix, which collectively promote cell attachment, gas exchange, and moisture management critical for wound healing [11–13]. These nanofibers are often biocompatible and can incorporate bioactive agents for controlled drug release, enhancing antimicrobial properties and tissue regeneration [14, 15]. Additionally, the electrospinning process allows customization of fiber morphology and composition to meet specific clinical needs [9, 16]. However, certain limitations persist, such as insufficient mechanical strength compared to conventional dressings, sensitivity of the production process to environmental conditions, limited solubility of some polymers, and higher production costs [16–18]. Recent studies have explored innovative solutions to address these challenges. For instance, biodegradable nanofiber scaffolds incorporating carbon quantum dots have demonstrated enhanced wound healing efficiency [14], while electrospun burn dressings with high porosity and drug-loading capabilities show promise in managing burn wounds [12, 19]. Another study highlights the antimicrobial effectiveness of functionalized electrospun nanofibers in wound care applications [15]. Despite their limitations, ongoing advancements in electrospinning technology continue to enhance the efficacy and applicability of nanofiber-based wound dressings in clinical settings.

Various natural and synthetic polymers are employed to fabricate electrospun nanofibers. However, it could be benifical if a new hybrid structure based on familiar FDA approved polymers could be designed. Polycaprolactone (PCL), Polyvinyl Alcohol (PVA), and Chitosan (CS) are widely used biopolymers in wound healing due to their unique properties. PCL is biodegradable, biocompatible, and offers excellent mechanical strength and flexibility, though its low hydrophilicity and slow degradation rate can limit interaction with biological fluids and potentially create acidic byproducts during degradation [20, 21]. PVA is highly hydrophilic, biocompatible, and forms strong films ideal for hydrogels, but excessive moisture retention may lead to bacterial infections, and its mechanical strength is lower compared to PCL [22, 23]. Also, CS, a naturally derived polymer, is biocompatible, biodegradable, and antimicrobial, promoting cell migration and wound healing; however, it has solubility issues in neutral pH and limited mechanical strength unless combined with other materials like PVA or PCL [24, 25]. When applied to wounds, PCL provides structural support with gradual degradation, PVA retains moisture for a hydrated healing environment, and CS prevents infections while enhancing cell proliferation [20, 22]. Compared to other biopolymers like gelatin or alginate, these materials offer superior mechanical strength, antimicrobial activity, and tailored properties for wound care [21, 23, 25]. The design of layered wound dressings using PCL as the layer ensures structural integrity and prolonged support, while the PVA/CS layer combines moisture retention with antimicrobial benefits to create a multifunctional dressing suitable for dynamic wound environments [24, 25].

Also, the polymeric core coated by an outer polymeric shell allows for encapsulating and controlling the release of drugs and biomolecules [26]. The core-shell nanofiber structure offers significant advantages for drug delivery, tissue engineering, and filtration. This design allows for the encapsulation of sensitive biomolecules, such as drugs or proteins, within the core, while the shell provides a protective barrier that preserves bioactivity and enables controlled release. By selecting specific materials for the core and shell, researchers can enhance properties like hydrophilicity, mechanical strength, and biodegradability. Additionally, core-shell fibers improve mechanical stability and surface-area-to-volume ratio compared to monolithic fibers, facilitating better adsorption and catalysis. These features highlight the potential of core-shell nanofibers in advancing material functionalities in biomedical applications [27, 28].

In addition to scaffolds, the employment of natural compounds, particularly biopharmaceuticals with great potential in wound healing has gained much attention. The bioactive molecules obtained from animal and plant sources have excellent anti-inflammatory, antibacterial, and collagen synthesis-inducing properties in favor of tissue repair and regeneration [29]. Squalene (SQ) is a triterpene with $C_{30}H_{50}$ formula produced in animals, plants, and fungi as an intermediate metabolite in the biosynthesis of sterols like cholesterol and steroid hormones [30]. SQ is the major compound

extracted from the nonsaponificable fraction of virgin olive oil (VOO) [31].

Recent studies have demonstrated the beneficial effects of SQ in wound healing and skin tissue regeneration. SQ enhanced anti-inflammatory cytokines, like IL-10, IL-13, and IL-4, in M1 proinflammatory macrophages and reduced proinflammatory TNF-α and NF-κB [31]. It also accelerated collagen deposition, revascularization, and macrophage polarization in the full-thickness burn wound model, indicative of increased tissue regeneration [32].

However, the architecher of designed structure is still important. The rationale for electrospinning a core-shell structure with polycaprolactone (PCL) as the shell and chitosan/polyvinyl alchol as the core lies in the unique advantages this configuration offers. PCL, known for its superior mechanical strength and flexibility, provides structural integrity and durability to the nanofibers, making it suitable as an outer layer [33–35]. Additionally, the core-shell arrangement facilitates the controlled release of bioactive agents encapsulated within the chitosan core, ensuring sustained therapeutic effects while maintaining the protective properties of PCL [35, 36]. The interaction between PCL and chitosan through hydrogen bonding enhances the stability of the nanofibers during electrospinning, preventing phase separation and ensuring uniformity in fiber morphology [37–39]. Furthermore, although chitosan is located in the core, post-processing techniques such as plasma treatment can modify the surface properties of PCL to improve cell interaction without compromising its mechanical benefits [40–42]. This configuration balances the strengths of both polymers, offering a promising approach for applications requiring controlled release and structural resilience.

This study introduces a hybrid scaffold composed of Poly(ε-Caprolactone) (PCL), Polyvinyl Alcohol (PVA), and Chitosan (CS), integrated with squalene, a natural compound recognized for its beneficial properties in wound healing. The incorporation of squalene not only enhances the scaffolds' anti-inflammatory and antioxidant capabilities but also represents a novel approach in utilizing squalene-loaded nanofibers specifically for this purpose. The electrospinning technique employed in the fabrication of these scaffolds results in highly porous structures that facilitate cell attachment and nutrient exchange while allowing for controlled release of squalene at the wound site. Furthermore, the in vivo evaluation conducted in this study provides essential insights into the scaffolds' effectiveness in biological environments, demonstrating their superior mechanical properties, biocompatibility, and enhanced healing outcomes compared to existing wound care materials.

Materials and Methods

Materials

The materials used in this study include Squalene (CAS-NO:111-02-4, Purity: ≥98%) Polyvinyl Alcohol (PVA,87–89% Hydrolyzed, Purity: 99%) with a molecular weight of 89–98 kDa (Catalog #341584, 99%), Sodium Quinate (SQ, Catalog #S3626, Purity: 99%), Polycaprolactone (PCL, Purity: 98%) with a number-average molecular weight of 80 kDa (Catalog #440744), and Chitosan (Cs) with a molecular weight of 100 kDa and a deacetylation degree of 93% (Catalog #900342, Purity: 99%), as well as beta-Glycerophosphate Disodium Salt Pentahydrate Calbiochem (CAS-NO:13408-09-8, Purity: ≥98%) all sourced from Sigma-Aldrich, Germany. Additionally, Dulbecco's Modified Eagle Medium (DMEM, Catalog #11–885-084, High Quality Cell Culture grade) and fetal bovine serum (FBS, Catalog #17934731, High Quality Cell Culture grade) were procured from Gibco Invitrogen. Furthermore, antibiotics such as penicillin (High Quality) and streptomycin (High Quality), along with trypsin/EDTA (High Quality Cell Culture grade), 3-(4,5-dimethylthiazole-2-yl)−2,5-diphenyltetrazolium bromide (MTT, Purity: 99%), and Dimethyl Sulfoxide (DMSO, Cell Culture grade, Purity: 99%), were obtained from Merck. NIH/3T3 is a fibroblast cell line that was isolated from a mouse NIH/Swiss embryo (Purity: Not Applicable) were acquired from the Pasteur Institute of Iran.

Scaffold Fabrication

Electrospinning of of PCL-PVA/Cs Hybrid Nanofibers

In the present experiment, blank and SQ-loaded PVA/Cs and PCL solutions were prepared according to the following instructions. PVA (MW: 89–98 KDa, Cat# 341584, Sigma-Aldrich, Germany) and Cs (MW: 100 KDa, deacetylation degree: 93%, Cat# 900342, Sigma-Aldrich, Germany) solutions were provided separately at 9% (w/v) and 2% (W/V) ratios by dissolving solid materials in deionized water (DW) and 1% (V/V) acetic acid, respectively, and then mixed at the 8:2 ratio. Various concentrations (0, 1, 2, 3, and 4% V/V) of SQ (Cat# S3626, Sigma-Aldrich, Germany) were added to the PVA/Cs mixture. 10% (W/V) PCL solution (Mn: 80 KDa, Cat# 440744, Sigam-Aldrich, Germany) was prepared by dissolving solid PCL in methanol/chloroform solution (1:1).

Brifly, PCL-PVA/Cs hybrid nanofibers were fabricated using a hybrid electrospinning method described elsewhere [43]. Blank and SQ-loaded PVA/Cs and PCL solutions were poured into 10 mL (G18) core and shell syringes bearing

stainless steel blunt needles in the electrospinning machine (Fnm. Co. Iran). The solution flow rate was adjusted at 0.7 mL/hour, where the needle-collector distance was 160 mm, and the electrical voltage of 21 kV was applied.

Scaffold Characterization

Fourier Transform Infrared Spectroscopy (FTIR)

The scaffold chemical characteristics were evaluated using the FTIR (Nicolet iS10 FTIR spectrometer, USA), where the spectra were collected as 100 scans in average at 400–4000 cm^{-1} with the resolution of 0.4 cm^{-1} at 400–4000 cm^{-1}.

Scanning Electron Microscope (SEM)

The scaffold morphology was assessed by visualizing gold-sputter-coated samples in an SEM machine (TESCAN ORSAY HOLDING, Brno-Kohoutovice, Czech Republic) at an accelerating voltage of 20 kV. The mean diameter of nanofibers was computed using Image J software (National Institute of Health, USA).

Degradation Measurement

Pre-weighted scaffolds were immersed in phosphate-buffered saline (PBS, pH = 7.4) and incubated at 37° C for 1, 4, 7, 14, and 28 days. At each time, scaffolds were rinsed in DW, dried in the oven at 40° C, and re-weighted. The degradation rate was calculated according to the following equation:

$$Degradation\ rate\ (\%) = \frac{W_0 - W_t}{W_t} \times 100$$

W_0 is the scaffold's dry weight before incubation, and W_t is the weight of the scaffold after incubation at the time t.

Swelling Measurement

Pre-weighted scaffolds were incubated in PBS for 1, 3, 5, 7, 14, and 20 h at room temperature. The water uptake ratio was computed following the below equation:

$$Swelling\ (\%) = \frac{W_w - W_d}{W_d} \times 100$$

W_d is the scaffold's dry weight, and W_w is the weight of the scaffold immersed in PBS.

Contact Angle

The nanofiber surface hydrophilicity was evaluated using a contact angle measurement device (CA-500 A, Sharif Solar Co. Iran) to measure the contact angle (θ) between water and the nanofiber surface.

In Vitro SQ Release

Specimens of PCL-PVA/Cs/SQ were weighed and subsequently immersed in phosphate-buffered saline (PBS) at a pH of 7.4, maintained at 37 °C with gentle agitation for durations of 1, 5, 10, and 14 days. At each time point, half of the PBS solution was removed and replaced with an equal volume of fresh PBS. The absorbance of the resulting supernatant was measured at 220 nm using a UV/Visible spectrophotometer (UNICO, Dayton, NJ, USA). The release of SQ was quantified by referencing a standard SQ calibration curve.

Tensile Strength Measurement

The tensile strength of the scaffolds was evaluated using a tensile testing machine (Instron UK model 3345 Single Column Testing System). In this assessment, a load cell with a capacity of 10 N was employed, applying a constant speed of 2 mm/min to the samples. The dimensions of the tested specimens were 50 × 10 mm^2, with a thickness of 64 µm and an area of 0.64 mm^2. All experiments were conducted in accordance with the ASTM D882 standard based on other researcher methods [44–46], which outlines the procedures for determining the tensile properties of thin plastic sheeting.

Biological Evaluations

Cell Line Preparation and Culture NIH/3T3 is a fibroblast cell line was purchased from the Pasteur Institute of Iran (Tehran, Iran) and cultured in the DMEM medium (Cat# 11–885-084, Gibco Invitrogen) enriched with 10% fetal bovine serum (FBS, Cat# 17934731, Gibco Invitrogen), 100 units/mL of penicillin, and 100 µg/mL of streptomycin at 37° C and 5% CO_2 pressure. After cells reached 80% confluency, they were detached using 0.25% trypsin/EDTA solution, centrifuged at 1800 rpm for 10 min, and subcultured.

Biocompatibility Assessment Before cell seeding, blank and SQ-loaded PCL-PVA/Cs scaffolds were cut into 5 × 5 mm^2 pieces and sterilized by subjecting them to ultraviolet (UV) irradiation for 20 min. NIH/3T3 is a fibroblast cell line were subjected to trypsinization and subsequently seeded

onto sterile scaffolds located at the bottom of a 96-well plate, achieving a cell density of 1 × 10^4 cells per well. The cells were cultured in complete DMEM for durations of 24, 48, and 72 h. At each time point, the culture medium was replaced with MTT solution (0.5 mg/ml, 200 µl per well) (Cat# M6494, Gibco Invitrogen), and the plate was incubated at 37 °C for three hours. Following incubation, the MTT reagent was removed, and 200 µl of DMSO was added to dissolve the formazan crystals. The optical density (OD) of the samples was then measured at 570 nm using an ELISA reader (Biorad, Hercules, CA, USA). Cell proliferation was calculated using the following equation:

$$Cellproliferation(\%) = \frac{OD_t}{OD_c} \times 100$$

ODc represents the absorbance of the PCL-PVA/Cs scaffold (control), while ODt denotes the absorbance of the PCL-PVA/Cs/SQ scaffolds.

Cell Attachment To examine the morphology and adhesion of cells cultured on the scaffold, the cells were fixed onto the scaffold surface to facilitate imaging using scanning electron microscopy. A 4% glutaraldehyde solution was used to fix the cells on the scaffold. Initially, approximately 5000 NIH3T3 fibroblast cells were seeded onto the scaffold and incubated for 3 days at 37 °C. The culture medium surrounding the samples was removed, and the samples were washed with phosphate-buffered saline. Subsequently, the 4% glutaraldehyde solution was applied to the scaffolds. After one hour, the glutaraldehyde solution was removed, and the samples were washed with a graded series of ethanol solutions (20–100%), each for 20 min. Finally, the samples were left to dry under a hood for 2 h. After confirming that the samples were dry, they were coated with a layer of gold and then imaged using scanning electron microscopy.

In Vivo Study

Wound Model and Experimental Group Design

This study was conducted following the guidelines of the Ethics Committee of Fasa University of Medical Sciences, Fasa, Iran [Ethics code: I.R.FUMS.AEC.1401.006].In vivo experiments were carried out according to the guidelines of the ethical committee of the Fasa University of Medical Sciences [Ethical code: IR.FUMS.AEC.1401.006], and reported following the ARRIVE guideline. The blank and SQ-loaded scaffolds were implanted into a full-thickness wound model for 5, 10, and 14 days. 6–8-week male Wistar rats were prepared from the Fasa University of Medical Sciences and housed at room temperature (25 ± 2°C) and 12-hour light-dark cycles with free access to food and water (n = 30). The animals were anesthetized by the intraperitoneal injection of ketamine (70 mg/kg) and xylazine (30 mg/kg), and excisions 2 × 2 cm^2 were made at the paravertebral region. 30 rats were divided into five experimental groups: (1) the control group (wounds covered with sterile gauze); (2) wounds treated with PCL-PVA/Cs (blank) scaffolds; (3) wounds implanted with PCL-PVA/Cs/SQ2% scaffolds; (4) wounds implanted with PCL-PVA/Cs/SQ3% scaffolds; (5) wounds implanted with PCL-PVA/Cs/SQ4%. The wound area was covered with scaffolds at 2.5 × 2.5 cm^2 dimensions [47], and then animals were returned to cages and monitored for likely complications, such as infections. In our study, mice underwent excision of three skin layers without splinting. Typically, superficial wounds allow for the observation of skin appendages during healing; however, our experimental groups showed no skin appendages (hair follicles, sebaceous glands, sweat glands) at the granulation and scar tissue sites. The new epidermis was thinner than that of adjacent healthy tissue, resulting in a concave wound appearance. Treatment groups were compared to a control group under identical conditions, and the methodology aligns with our previous research and that of others [47–52].

Wound Surface Area Assessment

On days 5, 10, and 14, macroscopic examination was performed to measure the wound surface area following the below equation [53]:

$$\%\ \text{wound closure} = \frac{\text{wound area (day 0)} - \text{wound area (particular day)}}{\text{wound area (day 0)}} \times 100$$

Histological Assessments

On day 14 post-implantation, animals were sacrificed by intraperitoneal injecting thiopental (90 mg/100 g body weight), and the wound areas bearing implanted scaffolds were excised for histopathological analyses. The tissue samples were fixed in 10% formaldehyde, dehydrated in ascending ethanol (60–96%), and embedded in paraffin blocks. Then, 5 µm tissue sections were prepared from tissue blocks, stained with hematoxylin-eosin (H&E) and Masson's trichrome (MT) and observed using a light microscope (Olympus CX 21) carrying a digital camera (TrueChrome II). Specimens were histologically examined for inflammatory cell infiltration, granulation tissue formation, collagen deposition, and re-epithelialization. The histopathological

Table 1 Correlation between qualitative histological observations and their conversion into quantitative scores

No	Score	Granulation tissue			Fibrotic tissue
		Edema	Vascularity	Inflammation	
1	0	Not seen			Not seen
2	0–1	Slight			Slight
3	1	Mild			Mild
4	1–2	Mild to moderate			Mild to moderate
5	2	Moderate			Moderate
6	2–3	Moderate to marked			Moderate to marked
7	3	Marked			markedM
8	3–4	Moderately marked			Moderately marked
9	4	Very marked			Very marked

changes were qualitatively scored according to the Table 1 [48]:

Re-epithelialization was calculated according to the following equation [53]:

$$\%\,\mathrm{Re}-\mathrm{epithelialization} = \frac{\mathrm{A}}{\mathrm{B}} \times\ 100$$

In the equation, A is the neo-epithelium length from both lateral sides of the wound with (mm), and B is the wound width (mm).

Antibacterial Tests

The antibacterial effect of various prepared groups were evaluated against Staphylococcus aureus ATCC25923 (Gram-positive bacteria) and Escherichia coli ATCC25922 (Gram-negative bacteria) strains. Briefly, after an overnight culture of bacterium, a suspension was prepared equal to half Mac Farland turbidity and lawn onto Mueller Hinton Agar medium (Merk, Germany). Next, One square centimeter of nanofibers was placed on a blank disk and incubated an overnight. The growth inhibitory effects of various groups were assessed by the measurement of growth inhibition zone radius.

Statistical Analysis

Quantitative data were collected in triplicates and reported as mean ± SD. One-way analysis of variance (ANOVA) followed by Tukey's test was carried out in GraphPad Prism 8 software at the significant level of P-value ≤ 0.05.

Results

FTIR

FTIR data for Cs, PCL, PVA, SQ, PV/PCL/Cs, and SQ-loaded PVA/PCL/Cs nanofibers are shown in Fig. 1. Also, The main peaks of Cs were detected around 1320 cm^{-1}: amide III (C-N stretching), 1575 cm^{-1}: amine groups, and

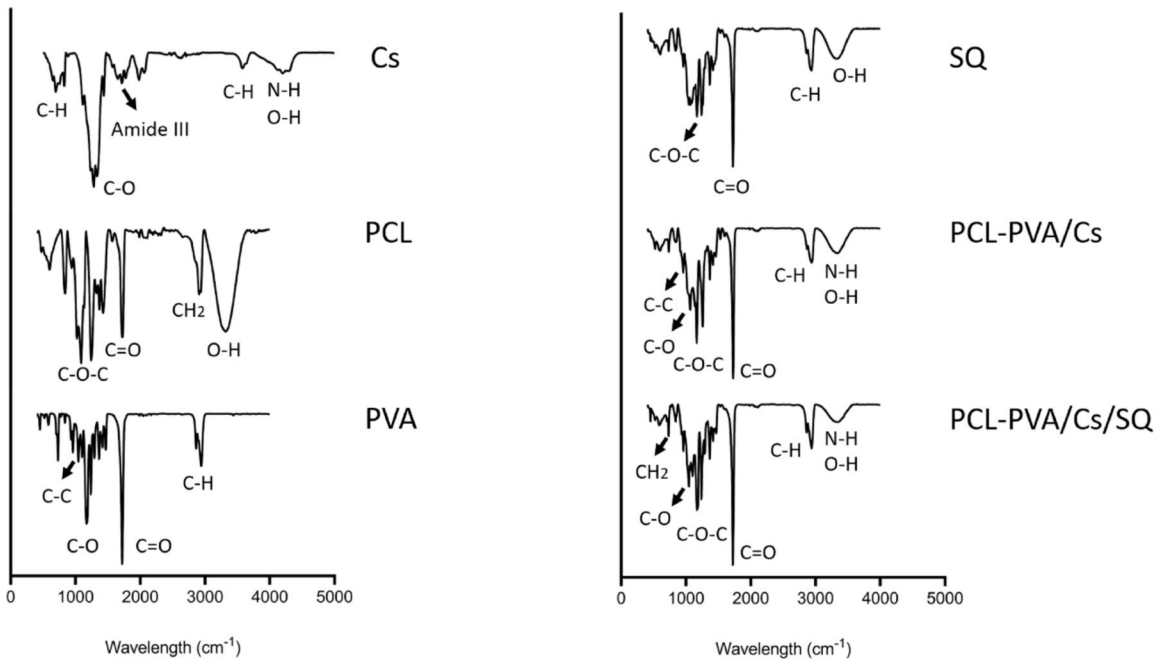

Fig. 1 FTIR spectra of Cs, PCL, PVA, SQ, PCL-PVA/Cs, and PCL-PVA/Cs/SQ scaffolds

1656 cm^{-1}: amide I (C=O stretching). The prominent peaks of PCL were observed at 1100–1240 cm^{-1}: C-O-C stretching, 1720 cm^{-1}: C=O stretching, and 2900–2960 cm^{-1}: CH_2 stretching. The peaks of PVA around 950–1200 cm-^{1} belonged to C-O and C-C stretching, and a peak at 1717 cm^{-1} stemmed from C=O stretching. Moreover, the peaks detected in the FTIR data of scaffolds included 952 cm^{-1}: C-C stretching (PVA), 1040 cm^{-1}: C-O stretching (PVA, Cs), 1250 cm^{-1}: C-O-C stretching (PCL), 1722 cm^{-1}: C=O stretching (PCL) and 3340 cm^{-1}: O-H and N-H stretching (Cs). Subsequently, the characteristic peaks of SQ were detected at 1166 cm^{-1}: CH3 scissoring bending, 1363 and 2940 cm^{-1}: C-H stretching. A detailed explanation for each spectrum is described in Table 2.

Table 2 The detailed description of FTIR spectra of Cs, PCL, PVA, SQ, PCL-PVA/Cs, and PCL-PVA/Cs/SQ scaffolds

Wavelength (cm^{-1})	Compound	Description
882.8	Cs	C-H bending of the aromatic ring
1020.2, 1068.7	Cs	Skeletal C−O stretching
1321.2	Cs	Amide III, C-N stretching
1371.7	Cs	Symmetrical deformation of CH_3 group
1575.8	Cs	Primary amine, N-H bending
1656.6	Cs	C=O stretching of Amide I
2868.7	Cs	C-H asymmetric stretching
3353.5	Cs	O-H and N-H stretching
1139	PCL	Symmetric C-O-C stretching
1240	PCL	Asymmetric C-O-C stretching
1366	PCL	O-H stretching
1722	PCL	C=O stretching
2906	PCL	Symmetric CH_2 stretching
2957	PCL	Asymmetric CH_2 stretching
3320	PCL	O-H stretching
950, 1166	PVA	C−C stretching
1042, 1166	PVA	C−O stretching
1358	PVA	CH_2 wagging
1717	PVA	C=O stretching
2863, 2936	PVA	Symmetric C−H stretching
1055	SQ	C-O-C stretching (ether group)
1166	SQ	CH_3 scissoring bending
1358	SQ	C-H stretching vibration
1722	SQ	C=O stretching vibration
2940	SQ	C−H stretching (triglyceride structure)
3320	SQ	O-H stretching
952	PVA/PCL/Cs	C−C stretching (PVA)
1040	PVA/PCL/Cs	C−O stretching (PVA, Cs)
1160	PVA/PCL/Cs	C−C and C-O stretching (PVA)
1252	PVA/PCL/Cs	Asymmetric C-O-C stretching (PCL)
1358	PVA/PCL/Cs	O-H stretching (PCL), CH_2 wagging (PVA)
1722	PVA/PCL/Cs	C=O stretching (PCL)
2936	PVA/PCL/Cs	Asymmetric C-O-C stretching (PCL), Symmetric C−H stretching (PVA)
3342	PVA/PCL/Cs	O-H and N-H stretching (Cs)
725	PVA/PCL/Cs/SQ	CH_2 rocking (SQ)
1050	PVA/PCL/Cs/SQ	C-O stretching (Cs)
1166	PVA/PCL/Cs/SQ	C−C and C-O stretching (PVA) CH_3 scissoring bending (SQ)
1244	PVA/PCL/Cs/SQ	Asymmetric C-O-C stretching (PCL)
1717	PVA/PCL/Cs/SQ	C=O stretching
1363	PVA/PCL/Cs/SQ	O-H stretching (PCL), CH_2 wagging (PVA) C-H stretching vibration (SQ)
2940	PVA/PCL/Cs/SQ	C−H stretching (SQ)
3320	PVA/PCL/Cs/SQ	O-H and N-H stretching

Morphology and Cell Attachment

SEM micrographs of both blank and SQ-loaded PVA/PCL/Cs scaffolds are presented in Fig. 2. The scaffold nanofibers exhibited smooth surfaces and were uniformly distributed in a random orientation without the presence of beads at SQ concentrations up to 2% (Fig. 2a). However, increasing the SQ content resulted in a non-uniform morphology characterized by the emergence of beads. The average diameters of the nanofibers, determined using Image J software (National Institutes of Health, Bethesda, USA), were 219 ± 33.4 nm, 227 ± 59.7 nm, 167.3 ± 35.9 nm, and 126.7 ± 39.75 nm for the PCL-PVA/Cs, PCL-PVA/Cs/SQ2%, PCL-PVA/Cs/SQ3%, and PCL-PVA/Cs/SQ4% scaffolds, respectively (Fig. 2c, d). Also, SEM was performed to examine cell adhesion to the scaffolds. These images indicate the adhesion of fibroblast cells onto the squalene-containing nanofibers, demonstrating that these cells maintain their morphology and adhere well to the surface of the aforementioned substrates (Fig. 2b). Analysis of the images revealed that squalene exhibits high biocompatibility and has a positive effect on the adhesion of fibroblast cells. In these studies, it was observed that upon seeding the aforementioned cells onto the nanofibrous scaffold containing 2% squalene, the cells adhered correctly to the surface of the nanofibrous scaffold, effectively promoting increased fibroblast cell growth and proliferation.

Degradation

The degradation rate of the scaffolds was determined based on weight loss over time (see Fig. 3a). The percentage of degradation for all scaffolds increased with prolonged incubation time (*** $P \leq 0.001$). Additionally, the scaffolds

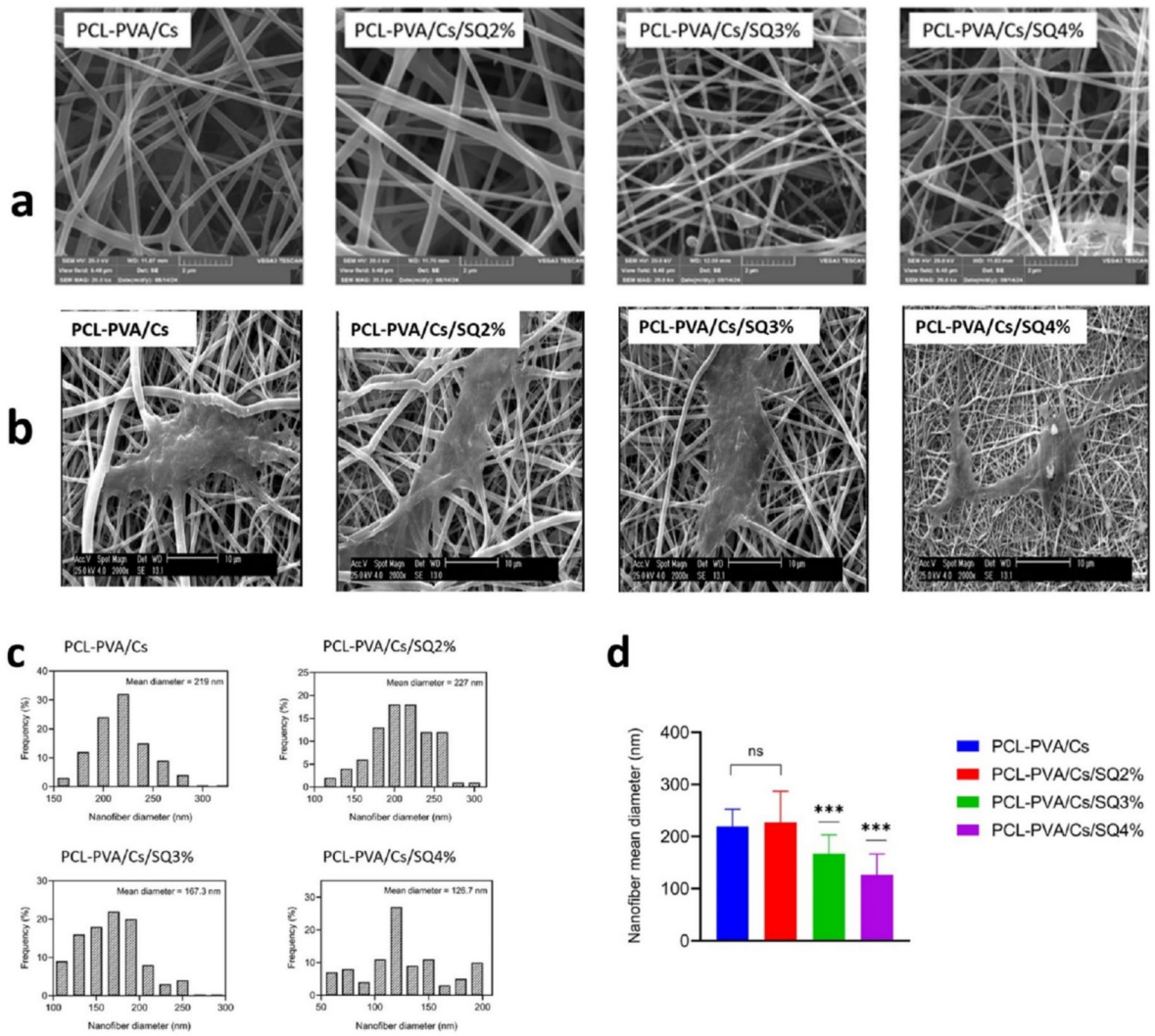

Fig. 2 Morphology and size analysis of hybrid nanofibers. (**a**) morphology of nanofibers (**b**) cell attachment on scaffolds (**c**) size distribution of samples. (**d**) average size of nanofibers. It was observed that increasing the concentration of SQ beyond 2% results in the formation of beads and a reduction in the average size of the nanofibers. (ns: none significant p-value = p, *$p \leq 0.05$, **$p \leq 0.01$, *** $p \leq 0.001$)

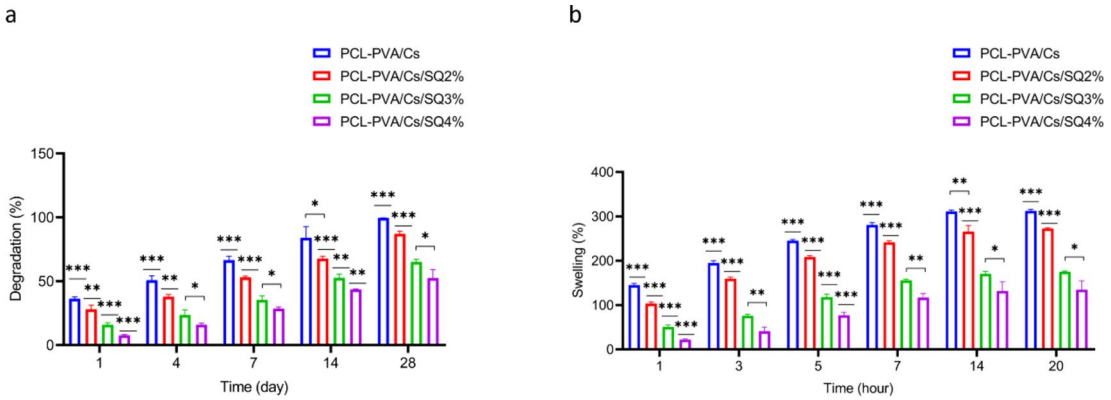

Fig. 3 Degradation and Swelling of Nanofiber Scaffolds (**a**) Degradation percentage, (**b**) Swelling percentage As anticipated, the scaffolds loaded with SQ exhibited a slower degradation rate and reduced swelling compared to the control group, which was dependent on the concentration of SQ. (ns: none significant p-value = p, *$p \leq 0.05$, **$p \leq 0.01$, *** $p \leq 0.001$)

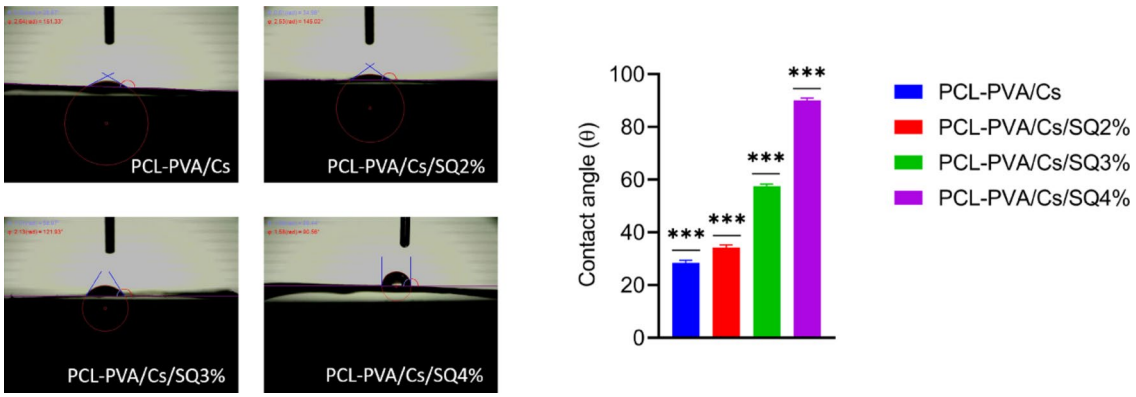

Fig. 4 Contact Angle of Nanofiber Scaffolds. The hydrophilicity of the scaffolds exhibited a notable decline as the content of SQ increased

loaded with SQ exhibited a slower degradation rate compared to the control group, which was dependent on the concentration of SQ (*** $P \leq 0.001$, ** $P \leq 0.01$, * $P \leq 0.05$).

Swelling

The potential of scaffolds to absorb water following immersion in PBS was measured up to 20 h (Fig. 3b). the results demonstrated that the swelling ratio enhanced in all scaffolds in a time-dependent manner (*** $P \leq 0.001$) while it declined in SQ-loaded scaffolds dose-dependently (*** $P \leq 001$, ** $P \leq 0.01$, * $P \leq 0.05$). The initial swelling ratio for control, SQ2%, SQ3%, and SQ4% scaffolds was 145.2 ± 3.7%, 103.4 ± 3.6%, 50.65 ± 4.4%, and 22 ± 1.8% which finally reached 312.3 ± 3.8%, 272.65 ± 1.6%, 175.2 ± 1.5%, and 134.6 ± 20.35%.

Contact Angle

The hydrophilicity of the scaffold surface was assessed using the contact angle measurement (Fig. 4). Θ values for control, SQ2%, SQ3%, and SQ4% scaffolds was 28.48 ± 0.92, 34.275 ± 0.96, 57.55 ± 0.76, and 90.148 ± 0.8. the data demonstrated that Θ values increased remarkedly depending on SQ concentration (*** $P \leq 0.001$). hydrophilicity of scaffolds decreased with increasing SQ content.

Mechanical Properties

The data of mechanical properties of scaffolds in tensile mood (Young's modulus, tensile strength, and stress-strain curve) is depicted in Fig. 5a-c, and Table 3. Results revealed that tensile strength, and Young modulus values of scaffolds were significantly intensified in SQ-loaded scaffolds compared with the control scaffold (***$P \leq 0.001$). Also, these parameters were magnified in an SQ dose-dependent manner with the highest mechanical strength, and modulus in PCL-PVA/Cs/SQ4% scaffolds (***$P \leq 0.001$). Moreover, the maximum strain of scaffolds were enhanced by increasing SQ content.

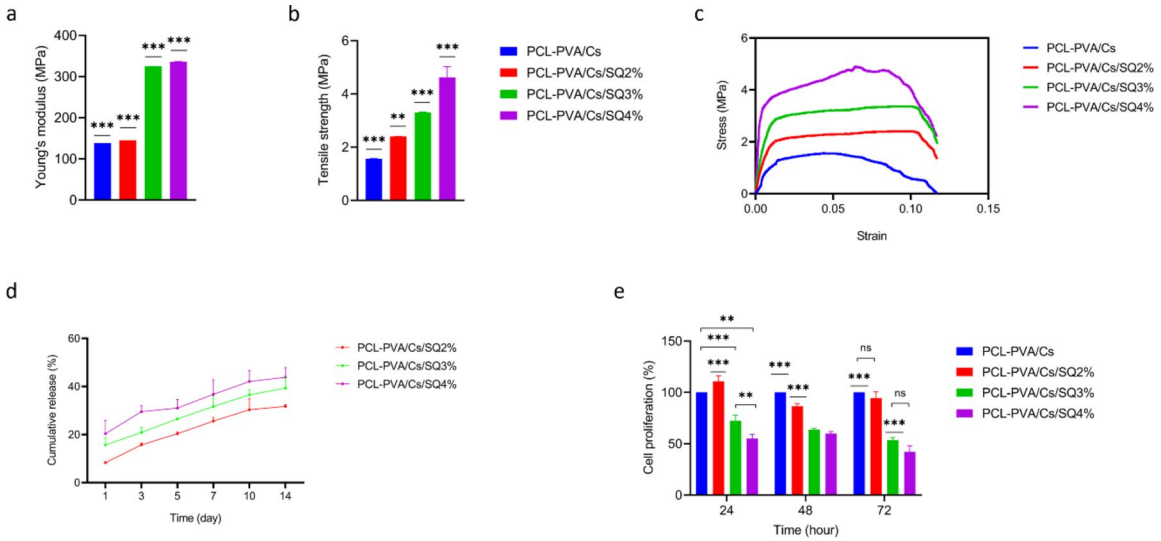

Fig. 5 Results of the mechanical properties, in vitro release of SQ, and cell viability of nanofibrous scaffolds. The results are categorized as follows: (**a**) Young's modulus, (**b**) tensile strength, (**c**) stress-strain curve, (**d**) in vitro SQ release, and (**e**) cell viability. The mechanical characteristics of the nanofibrous scaffolds were improved in a manner that was dependent on the concentration of SQ. Additionally, a sustained release of SQ from the scaffolds was noted. Among the various hybrid scaffolds tested, the PCL-PVA/Cs/SQ2% scaffolds demonstrated the highest levels of cell viability. (ns: none significant p-value = p, *$p \leq 0.05$, **$p \leq 0.01$, ***$p \leq 0.001$)

Table 3 Mechanical properties of nanofiber scaffolds. Tensile strength, Young's modulus, maximum strain of scaffolds were significantly increased with enhancing SQ content

Sample name	Tensile Strength (MPa)	Young's Modulus (MPa)	Max.Strain (%)
PCL-PVA/Cs	1.5643 ± 0.004	138.5067 ± 0.012	12.2727 ± 0.008
PCL-PVA/Cs/SQ 2%	2.4032 ± 0.006	145.3167 ± 0.012	20.3397 ± 0.013
PCL-PVA/Cs/SQ 3%	3.3318 ± 0.021	329.53 ± 1.087	27.0662 ± 0.035
PCL-PVA/Cs/SQ 4%	4.6202 ± 0.394	342.97 ± 2.741	30.0869 ± 0.002

In Vitro SQ Release

The release of SQ was assessed by incubating scaffolds in PBS at pH = 7.4 and 37° C for 14 days (Fig. 5d). The results showed that SQ was gradually released from scaffolds over time, and the amount of released SQ was directly correlated with the initial content of SQ incorporated into scaffolds (*** $P \leq 0.001$).

Cell Proliferation

The proliferation of fibroblasts seeded on scaffolds was assessed using the MTT assay at 24, 48, and 72 h (see Fig. 5e). At the 24-hour mark, cell proliferation was notably enhanced in the group with PCL-PVA/Cs/SQ2% scaffolds, while a decrease in proliferation was observed in the PCL-PVA/Cs/SQ3% and PCL-PVA/Cs/SQ4% groups. Statistically significant differences were identified among the various groups (*** $P \leq 0.001$, ** $P \leq 0.01$). At both the 48-hour and 72-hour intervals, a decline in cell proliferation was evident in the SQ-loaded scaffolds compared to the control scaffold, with this effect being dependent on the concentration of SQ. However, no significant differences were found between the PCL-PVA/Cs/SQ2% and PCL-PVA/Cs/SQ3% groups (*** $P \leq 0.001$, ns: non-significant). A closer examination of the data indicated that throughout all time points, the PCL-PVA/Cs/SQ2% scaffolds exhibited the highest cell viability when compared to the other hybrid scaffolds (PCL-PVA/Cs/SQ3% and PCL-PVA/Cs/SQ4%).

Wound Size Measurement

Wound dimensions were evaluated on days 0, 5, 10, and 14 post-implantation (refer to Fig. 6). The results indicated a significant decrease in wound size across all experimental groups over time (*** $P \leq 0.001$). Importantly, the reduction in wound size was more pronounced in the groups that received implanted scaffolds compared to the control group, with a particularly noteworthy decrease observed in the SQ-loaded scaffolds when compared to the blank group (*** $P \leq 0.001$, ** $P \leq 0.01$, * $P \leq 0.05$). Among all groups, the smallest wound area was noted in the PCL-PVA/Cs/SQ2% group (*** $P \leq 0.001$, ** $P \leq 0.01$).

Histological Assessments

Histological assessments were performed on day 14 post-implantation using H & E and MT staining (Fig. 7, and

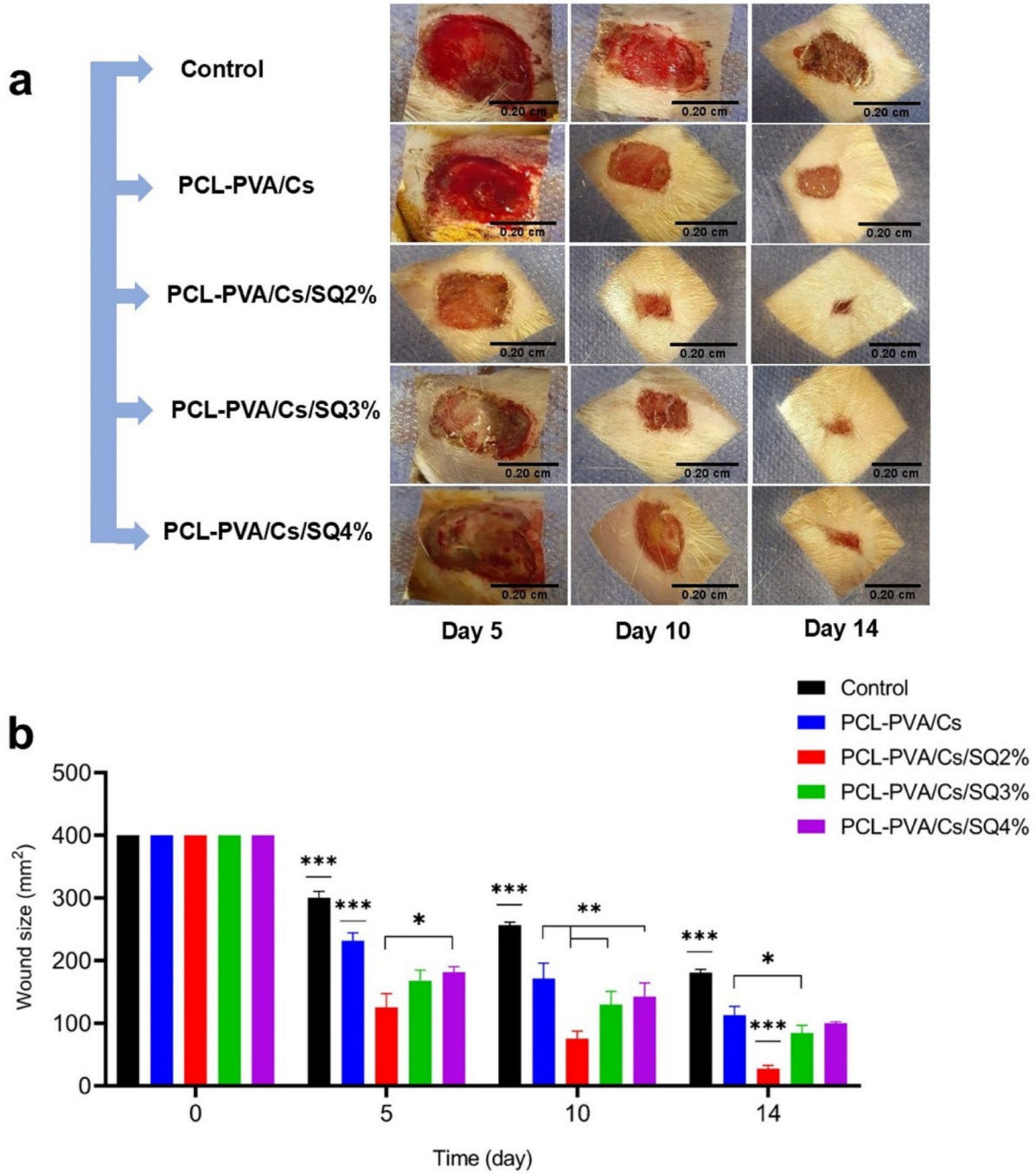

Fig. 6 Wound size progression in an animal model following scaffold implantation, observed on days 0, 5, 10, and 14. **a**) Macroscopic images of wounds from the Control, PCL-PVA/Cs, PCL-PVA/Cs/SQ2%, PCL-PVA/Cs/SQ3%, and PCL-PVA/Cs/SQ4% groups captured on days 5, 10, and 14. Among all groups, the PCL-PVA/Cs/SQ2% group consistently demonstrated the smallest wound size at all observed time points. **b**) Quantitative analysis of wound dimensions recorded on days 0, 5, 10, and 14 post-implantations. Scaffolds containing SQ showed enhanced efficacy in reducing wound size compared to the control group. Notably, the PCL-PVA/Cs/SQ2% scaffold exhibited the most significant reduction in wound area among all tested groups. (ns: not significant, p-value = p; *$p \leq 0.05$, **$p \leq 0.01$, ***$p \leq 0.001$)

Fig. 8) and a summary of histopathological parameters is presented in Table 4. In the control group, the long-lasting existence of scabs prevented re-epithelialization and fluid exudation associated with aggregation of loose fibrin, and moderate to high infiltration of acute inflammatory cells was observed. Low amounts of granulation tissue and collagen deposition, angiogenesis, and edema reflected early stages of tissue repair. In the PCL-PVA/Cs group, re-epithelialization wasn't observed, and middle-phase granulation tissue, moderate edema, angiogenesis, and collagen deposition associated with moderate to severe infiltration of chronic inflammatory cells indicated deficient tissue repair.

In the PCL-PVA/Cs/SQ2% group, re-epithelialization and stratum layer were completely formed. Edema, congested blood vessels, and inflammatory cells were significantly reduced compared to granulation tissue. MT staining revealed enhanced collagen and ECM deposition, indicative of fibrotic scar repopulated with aligned myofibroblasts. In the PCL-PVA/Cs/SQ3% group, the epithelial layer was formed but thinner than that of normal tissues. The loose granulation tissue, mild edema, and severe acute and chronic inflammation were detected in the surface layer. In the deeper layer, the moderate infiltration of chronic inflammatory cells and moderate to severe angiogenesis were visualized. Collagen and ECM deposition were negligible in the surface layer but increased in the deep layer, identified by the formation of fibrotic scars in the middle to late phases. In the PCL-PVA/Cs/SQ4% group, the thin epithelial layer was formed while early to middle granulation tissue, edema, congested blood vessels, and mild to moderate infiltration of chronic inflammatory cells were visible in the surface layers. Collagen and ECM deposition were higher in deep layers, reflecting the scar tissue in the middle to late stages.

Although the epidermis is almost formed, inflammatory granulation tissue and scar can be observed. The guide of symbols and letters in the figure is as follows: H: Hypodermis, D: Dermis, E: Epidermis, SC: Scab, HF: Hair follicle, SG: Sebaceous gland, ST: Scar tissue, REP: Re-epithelialization, Lm: Lymphocyte, Mo: Monocyte, Nu: Neutrophil, Ma: Macrophage, Fb: Fibroblast, Fc: Fibrocyte, MF: Myofibroblast, V: Vessel, RBC: Red blood cell, GT: Granulation tissue. The quantitative analysis of histopathological assessments is shown in Fig. 9. Re-epithelialization, collagen deposition, and fibrosis parameters improved upon wound healing. Edema was lower in PCL-PVA/Cs/SQ scaffolds than in the control group, but a significant decrease was observed in PCL-PVA/Cs/SQ2% (* $P \leq 0.05$) (Fig. 9a). Inflammatory manifestations notably declined in SQ-loaded scaffolds, with the highest fall in the PCL-PVA/Cs/SQ2% group (** $P \leq 0.01$, * $P \leq 0.05$) (Fig. 9b).

The intensity of blood vessel formation fell off in PCL-PVA/Cs/SQ groups, where the PCL-PVA/Cs/SQ2% exhibited the highest impact (*** $P \leq 0.001$, * $P \leq 0.05$) (Fig. 9c). The formation of fibrotic tissue, evaluated by collagen deposition, expanded in SQ-loaded scaffolds; however, statistical differences were observed between the PCL-PVA/Cs/SQ2% group with the control and PCL-PVA/Cs groups (*** $P \leq 0.001$, * $P \leq 0.05$) (Fig. 8d). The thickness of newly-formed epithelium showed an outstanding increment in SQ-loaded scaffolds, and the epithelial layer had the highest thickness in PCL-PVA/Cs/SQ2% groups (*** $P \leq 0.001$) (Fig. 8e).

Antibacterial Tests

The antibacterial properties of various groups unveiled more potent effects by nanofibers containing higher concentrations of SQ of 4% and 3% and 2% (Fig. 10a-h). Accordingly, Cs/BG-SQ4% had inhibitory zone of 30 mm (Fig. 9h) against S. aureus ATCC25923 and 22 mm (Fig. 10d) against E. coli ATCC25922. It was followed by Cs/BG-SQ3% (24 mm against S. aureus and 20 mm against E. coli, Fig. 10g and c), Cs/BG-SQ2% (23 mm and 18 mm, respectively, Fig. 9F and B). Notably, free nanofibers had no inhibitory zone (2 mm, Fig. 10a and e).

Discussion

Wound healing, particularly for chronic wounds, presents significant challenges for both patients and healthcare providers [54]. To enhance healing quality and reduce recovery time, various strategies have been explored, including tissue engineering that utilizes engineered scaffolds, stem cells, and growth factors [55, 56]. Scaffolds made from natural polymers like chitosan, alginate, and collagen exhibit promising results. However, the advantages of synthetic polymers such as polyvinyl alcohol (PVA) and polycaprolactone (PCL) have led to the development of hybrid scaffolds that combine both natural and synthetic materials [57]. Nanofiber scaffolds are particularly noteworthy due to their resemblance to the extracellular matrix (ECM) of skin tissue, which is primarily composed of collagen fibers. This biomimetic approach aids in creating effective wound dressings [58, 59]. Additionally, continuous drug delivery systems incorporated into scaffolds can significantly enhance wound healing [60]. Scaffolds loaded with biologically derived drugs, such as those from thyme or squalene, show great potential in accelerating the healing process [47, 61, 62]. In summary, advancements in scaffold design—particularly through the integration of natural and synthetic materials—along with innovative drug delivery methods, are paving the way for improved treatments in wound healing. The combination of these technologies holds promise for

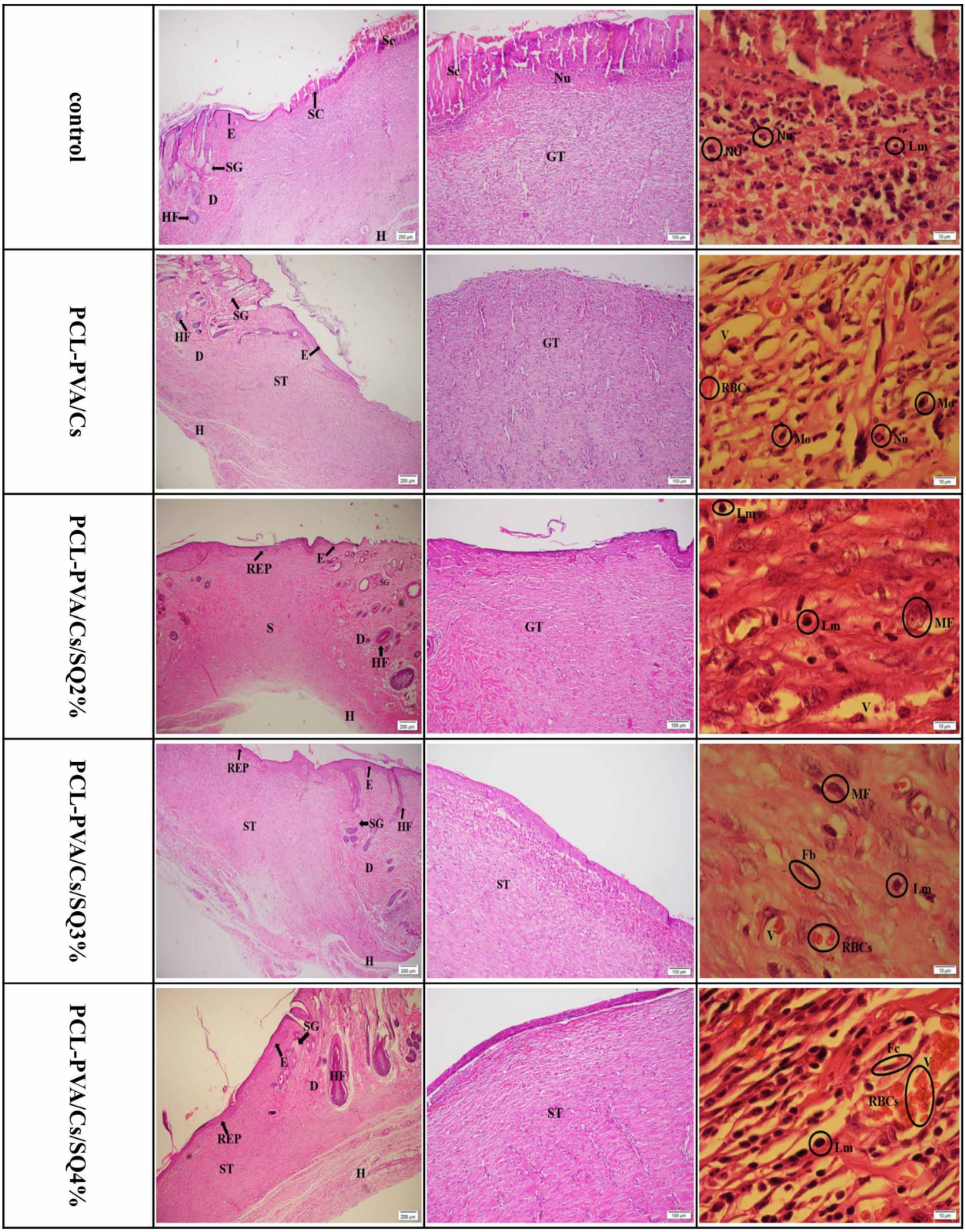

addressing the complexities associated with chronic wounds and enhancing patient outcomes.

Hence, in the present study, we fabricated electrospun hybrid PCL-PVA/Cs scaffolds loaded with SQ and evaluated their effect on wound healing in full-thickness wound

Fig. 7 Hematoxylin-eosin (H&E) staining in the control group and scaffold-containing groups. In the Control group, the prolonged presence of the scab hindered re-epithelialization, with underlying exudation of fluid accompanied by loose fibrin accumulation and moderate acute inflammation, alongside minimal granulation tissue, indicating the early stages of healing (40X, 100X, and 1000X). The PCL-PVA/Cs group also did not demonstrate re-epithelialization, showing moderate granulation tissue and significant chronic inflammation, which indicates inadequate healing (40X, 100X, and 1000X). In the PCL-PVA/Cs/SQ2% group, complete re-epithelialization occurred, with reduced edema indicating more effective tissue repair (40X, 100X, and 1000X). The PCL-PVA/Cs/SQ3% group exhibited a thinner epithelial layer, mild edema, and persistent inflammation (40X, 100X, and 1000X). Finally, the PCL-PVA/Cs/SQ4% group displayed a thin epithelial layer along with granulation tissue in deeper layers (40X, 100X, and 1000X). The legend for the symbols and abbreviations used in the figure is as follows: H: Hypodermis, D: Dermis, E: Epidermis, SC: Scab, HF: Hair follicle, SG: Sebaceous gland, ST: Scar tissue, REP: Re-epithelialization, Lm: Lymphocyte, Mo: Monocyte, Nu: Neutrophil, Ma: Macrophage, Fb: Fibroblast, Fc: Fibrocyte, MF: Myofibroblast, V: Vessel, RBC: Red blood cell, GT: Granulation tissue

models. Hybrid electrospun nanofibers are promising candidates in skin tissue engineering since they are similar to the fibrous compartment of native ECM, providing an appropriate substrate for cellular attachment and survival [63]. Also, the core structure enables the incorporation and delivery of various bioactive compounds to the defect site, enhancing their therapeutic potential and tunable release [26]. FTIR analyses (Fig. 1; Table 2) confirmed the presence of SQ in the scaffold matrix, where the SQ peaks overlapped with those of scaffold components, leading to peak augmentation. Also, SQ incorporation resulted in the slight shift of FTIR peaks into the lower wavelengths [64].

Morphological observations (Fig. 2) showed scaffolds shared uniform nanofibrous architecture with smooth surfaces without beads and nanometric dimensions less than 250 nm. Electrospun nanofibers ranging from 50 to 500 nm mimic that of native ECM collagen, suited for tissue engineering applications [65]. All nanofibers were arranged unaligned randomly, proposed to facilitate gas exchange, oxygen permeation, and cell proliferation [66]. The nanofiber diameter increased in PCL-PVA/Cs/SQ2%, while a remarkable reduction was observed in scaffolds loaded with higher concentrations of SQ (3% and 4%), which might be due to a decrease in the viscosity of polymeric solution [67]. Also, desirable cell attachment was observed, in which can be associated to biocompatibility and bioactivity of squalene.

Moreover, Squalene exhibits notable surface-active properties, characterized by a surface tension of approximately 32 mN/m, which enables it to effectively reduce surface tension at the oil-water interface, akin to traditional surfactants [68, 69]. Recognized primarily as an emollient, squalene's ability to lower surface tension suggests its potential to enhance emulsion stability by improving the mixing of oil and water phases, making it a valuable component in cosmetic formulations where stability is essential [70–73]. The incorporation of squalene as a emollient in which has similarity to surfactants significantly reduces the diameter of electrospun fibers through several mechanisms. It decreases the surface tension of the polymer solution, facilitating finer jet formation during electrospinning and allowing for more efficient stretching and thinning of the solution, which results in smaller fiber diameters [74–76]. Additionally, squalene may enhance jet stability by preventing premature breakup, promoting controlled fiber formation and uniformity. Furthermore, emollients like squalene improve polymer chain mobility, aiding in better alignment during fiber formation and contributing to reduced fiber diameters. They also affect key electrospinning parameters such as voltage and flow rate, optimizing conditions for producing ultrafine fibers essential for applications in filtration and biomedical fields [77–81]. Previous studies have shown that larger nanofiber diameters allow for better drug encapsulation and release, characterized by an initial burst release followed by a long-term gradual release [82]. Nanofibers with smaller diameters share a higher surface area-to-volume ratio, which is advantageous for cell attachment and metabolism [83].

Degradation is a key aspect of tissue engineering scaffolds because the gradually- degrading scaffolds provide temporary support for cellular attachment, survival, and migration while allowing for tissue regeneration and integration [84]. Synthetic polymers like PCL and PVA mainly undergo hydrolysis, while natural ones like Cs break down following enzymatic reactions [85]. Our findings (Fig. 3a) showed that all scaffolds degraded over time in vitro; however, PCL-PVA/Cs/SQ scaffolds displayed slower degradation, relying on SQ concentration. We proposed that incorporating SQ, due to long hydrocarbon chains and hydrophobic nature, limited the scaffold interactions with the aqueous environment, reducing the degradation rate [86].

Also, Scaffold swelling (Fig. 3b) is prominent in tissue engineering because it makes gas exchange and nutrient transport easier in the biological milieu, which is favored for cellular metabolism and tissue growth [87]. Our results indicated that PCL-PVA/Cs scaffolds had the highest swelling ratio, with approximately 150% initial increment reaching > 300% at the end of incubation. In contrast, SQ-loaded scaffolds exhibited a diminished swelling ratio, dependent on SQ concentration. PCL-PVA/Cs/SQ2% nanofibers offered higher swelling than other SQ-loaded groups. In addition to the swelling, scaffold wettability is a crucial factor reflecting desirable cell-scaffold interactions; such hydrophilic surfaces layout better protein adsorption and cell attachment [88].

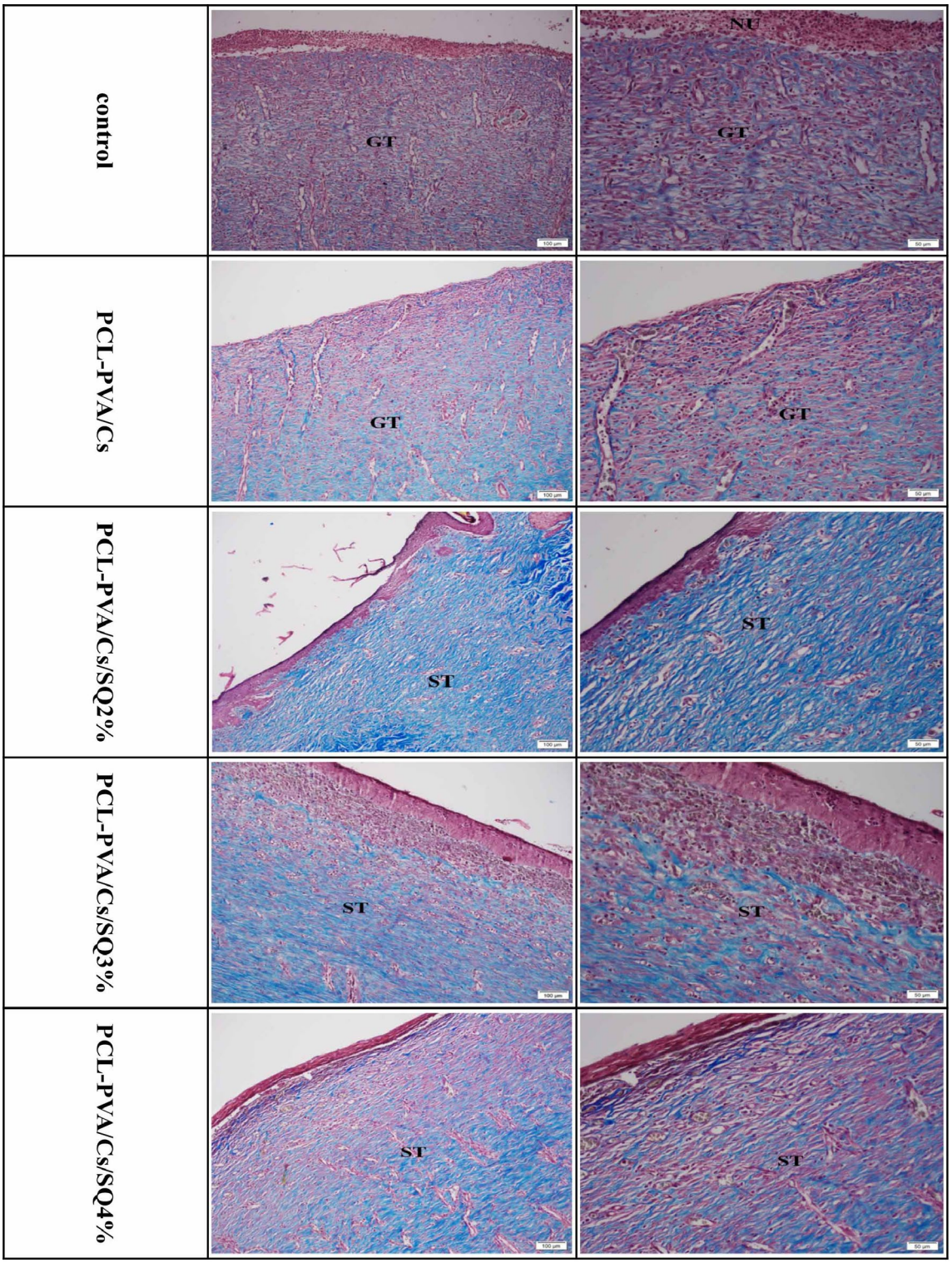

It has recently been suggested that wettability is more influential than surface morphology in guiding cellular behavior on electrospun nanofibrous scaffolds [89]. We evaluated scaffold wettability (Fig. 4) by calculating contact angle (Θ), and the results intimated that PCL-PVA/Cs and PCL-PVA/Cs/SQ2% possessed Θ values ranging 20–40°, corresponding to hydrophilic surface. Θ values of PCL-PVA/Cs/SQ3% scaffolds were approximately 60°, indicating moderate wettability, while PCL-PVA/Cs/SQ4% owned Θ values 90°, attributed to hydrophobic surfaces. Previous literature suggested that surfaces with Θ values ranging from 40–70° are optimal for cell adhesion [90]. These

Fig. 8 Masson's trichrome staining in the control and scaffold-containing groups. In the control group, minimal matrix and collagen fibers are observed within the connective tissue, appearing blue, with no conversion of granulation tissue to fibrotic scar tissue (200X and 100X). The PCL-PVA/Cs group shows low to moderate deposition of the extracellular matrix and collagen content, indicating incomplete healing (200X and 100X). In the PCL-PVA/Cs/SQ2% group, increased deposition of the extracellular matrix and collagen fibers in the connective tissue indicate the formation of fibrotic scar tissue, with effective tissue repair (200X and 100X). The PCL-PVA/Cs/SQ3% group shows increased deposition of the extracellular matrix and collagen fibers in the deeper layers, indicative of fibrotic scar tissue in the mid-to-late phase, which appears blue (200X and 100X). Finally, the PCL-PVA/Cs/SQ4% group exhibits a thin epithelial layer along with early granulation tissue and increased collagen deposition in the deeper layers, reflecting ongoing scar formation (200X and 100X). The legend for the symbols and abbreviations used in the figure is as follows: H: Hypodermis, D: Dermis, E: Epidermis, SC: Scab, HF: Hair follicle, SG: Sebaceous gland, ST: Scar tissue, REP: Re-epithelialization, Lm: Lymphocyte, Mo: Monocyte, Nu: Neutrophil, Ma: Macrophage, Fb: Fibroblast, Fc: Fibrocyte, MF: Myofibroblast, V: Vessel, RBC: Red blood cell, GT: Granulation tissue

data manifested that enhanced hydrophobicity of SQ-loaded scaffolds, especially at higher SQ concentrations, was correlated to the hydrophobic structure of SQ [86].

The spectrophotometric analyses revealed that SQ was released moderately as a function of time, and the cumulative release elevated upon loading higher concentrations of SQ (Fig. 5d). Hybrid nanofibers entrap biomolecules in them, which is advantageous for sustained release and regulating cell signaling [91]. Mechanical strength is essential in improving cell proliferation and inducing differentiation into tissues of interest. Nanofibrous scaffolds could be adjusted to fulfill the tensile strength close to native human skin while maintaining cell survival and infiltration [92]. Young's modulus and tensile strength were expanded in PCL-PVA/Cs/SQ scaffolds as the SQ dose increased. This might arise from reduced nanofiber diameter, enlarging the surface area to volume ratio, and increasing intermolecular hydrogen bonds and polar interactions between the scaffold components (Fig. 5a-c) [93, 94].

We investigated the cytotoxic effect of scaffolds against fibroblast cells using the MTT assay (Fig. 5e). PCL-PVA/Cs and PCL-PVA/Cs/SQ2% scaffolds had no toxic effects on cell proliferation, while PCL-PVA/Cs/SQ3% and PCL-PVA/Cs/SQ4% scaffolds notably declined cell proliferation. The cytoprotective effect might be attributed to the antioxidant property of SQ and its role in reducing intracellular reactive oxygen species (ROS) levels [95]. Although the main mechanism of SQ in diminishing cell proliferation is not fully elucidated, high concentrations of anti-oxidants seem to induce excessive ROS generation, DAN damage, and cell cycle arrest in proliferating cells [96, 97].

Our histological evaluations (Figs. 7 and 8) showed that PCL-PVA/Cs/SQ2% scaffolds had the most eminent effect on wound healing, identified by reduced inflammatory reactions, higher collagen deposition contents, and the formation of full-thickness stratum epithelium. This trend has been corroborated through quantitative analyses of healing scores, as illustrated in Fig. 9, as well as assessments of wound size, depicted in Fig. 6. These analyses provide robust evidence supporting the observed patterns, highlighting the relationship between healing metrics and wound dimensions.

The trend observed in the present results has been confirmed by other researchers. For example, Shanmugarajan et al. revealed that squalene-loaded agar-based emulgel scaffolds accelerated wound contraction and improved collagen deposition, revascularization, keratinocyte proliferation, and macrophage polarization [32]. A possible mechanism of SQ in promoting wound healing is attributed to modulating macrophage polarization. Conventional M2 macrophages turn into M1 counterparts during wound healing, with anti-inflammatory effects contributing to tissue remodeling [98]. SQ accelerated the recruitment of phagocytic cells and M1 macrophage transition and prompted remodeling and repairing signals (TIMP-2), influencing wound healing [31].

Furthermore, angiogenesis is particularly prominent during the proliferative phase, where new capillaries invade the wound bed and form a microvascular network essential for granulation tissue formation. Moreover, macrophages release various angiogenic factors that further amplify this process, highlighting the dynamic interplay between immune response and vascular development [99, 100]. Hence, it seems that one of the mechanisms of effectiveness of SQ-loaded scaffolds could be its effects on angiogenesis [101].

Because, effective angiogenesis is vital for successful wound healing. It not only supports tissue repair but also influences scar formation. An excess of angiogenesis can lead to pathological conditions such as hypertrophic scars or keloids, while insufficient angiogenesis can result in chronic non-healing wounds [102, 103]. Therefore, understanding the balance of angiogenic processes is crucial for developing therapeutic strategies aimed at improving wound healing outcomes [46].

Also, the antibacterial analysis demonstrated that higher loading of SQ, leads to higher zone inhibition and as results higher antibacterial activity (Fig. 10). This result can be related to the fact that SQ appeared to own an intense antibacterial activity against various gram-positive and gram-negative bacteria, which could minimize adverse inflammatory responses and promote tissue repair [104]. Despite promising results obtained from PCL-PVA/Cs/SQ2% in vitro and in vivo, scaffolds loaded with higher amounts of SQ (3% and 4%) revealed fewer wound-healing effects. These findings coordinated with previous studies that discussed SQ

Table 4 A summary of histopathological parameters assessed in experimental groups on day 14 post-implantation

	Control	PCL-PVA/Cs	PCL-PVA/Cs/SQ2%	PCL-PVA/Cs/SQ3%	PCL-PVA/Cs/SQ4%
Edema	Mild to moderate	Slight to moderate	Slight	Mild to moderate	Slight to moderate
Inflammation	Moderate to marked	Mild to moderate	Slight	Slight to moderate	Slight
Vascularization	Mild to marked	Mild to moderate	Slight	Slight to moderate	Mild to moderate
Fibrotic tissue	Slight to moderate	Mild to moderate	Moderately marked	Mild to moderate to marked	Mild to moderate to marked

lost its anti-inflammatory and tissue-reparative characteristics at high concentrations [105].

However, this study has several limitations that require careful consideration. Firstly, while polycaprolactone (PCL), polyvinyl alcohol (PVA), and chitosan are generally biocompatible, their interactions within a hybrid scaffold need further investigation, particularly since PCL's degradation products may be acidic and hinder healing [20, 106, 107]. Although the study aims to enhance mechanical strength through material hybridization, the mechanical properties of PVA and chitosan may not provide sufficient structural integrity in dynamic wound environments [15, 108]. Additionally, the scaffolds' efficacy may be limited to specific wound types, such as full-thickness burns, raising concerns about the generalizability of findings to chronic or diabetic wounds [16, 17]. Furthermore, the in vivo evaluation may not adequately assess long-term effects beyond initial healing phases, neglecting factors like scar formation and long-term biocompatibility [109, 110]. More research is also needed to optimize squalene loading into nanofibers, which could influence its release profile and therapeutic efficacy [111, 112]. Lastly, despite employing various characterization techniques, more advanced methods like dynamic mechanical analysis (DMA) are necessary to evaluate scaffold properties comprehensively [113, 114]. Moreover, despite incorporating antimicrobial properties via chitosan and squalene, there remains a risk of bacterial colonization and biofilm formation, which is critical for successfulness in wound healing applications [115, 116]. Addressing these limitations is crucial for enhancing clinical relevance and ensuring effective patient outcomes in hybrid scaffold technology for wound healing.

Conclusion

Hybrid electrospun nanofibers made from PCL-PVA/Cs have shown considerable promise as scaffolds for wound dressings, significantly enhancing wound healing in vivo. The unique biomimetic structure of these hybrid nanofibers facilitates the localized delivery and controlled release of therapeutic agents, particularly SQ in this study, thereby enhancing their positive effects on tissue repair. Notably,

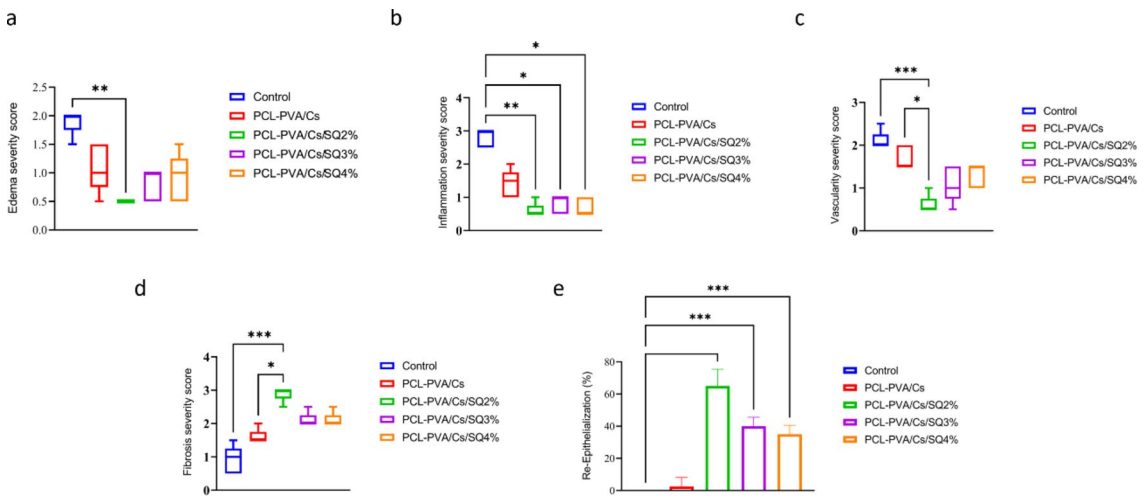

Fig. 9 quantitative analysis of histopathological assessments in the control group, scaffolds implanted groups. (**a**) Edema sensivity score, (**b**) Inflammatory sensivity score, (**c**) vascularity sensivity score, (**d**) Fibrosis sensivity score, (**e**) Re-epithelialization sensivity score. The quantitative analysis of histopathological evaluations indicates that wound healing improved with PCL-PVA/Cs/SQ scaffolds, particularly in the PCL-PVA/Cs/SQ2% group. Key findings include reduced edema levels and significant decreases in inflammatory responses, especially in the SQ-loaded scaffolds. Blood vessel formation was less extensive in these groups, with the most pronounced effects in the PCL-PVA/Cs/SQ2% group. Additionally, collagen deposition increased, and epithelial thickness significantly improved in SQ-loaded scaffolds, highlighting their effectiveness in promoting healing. (ns: none significant p-value = p, *$p \leq 0.05$, **$p \leq 0.01$, *** $p \leq 0.001$)

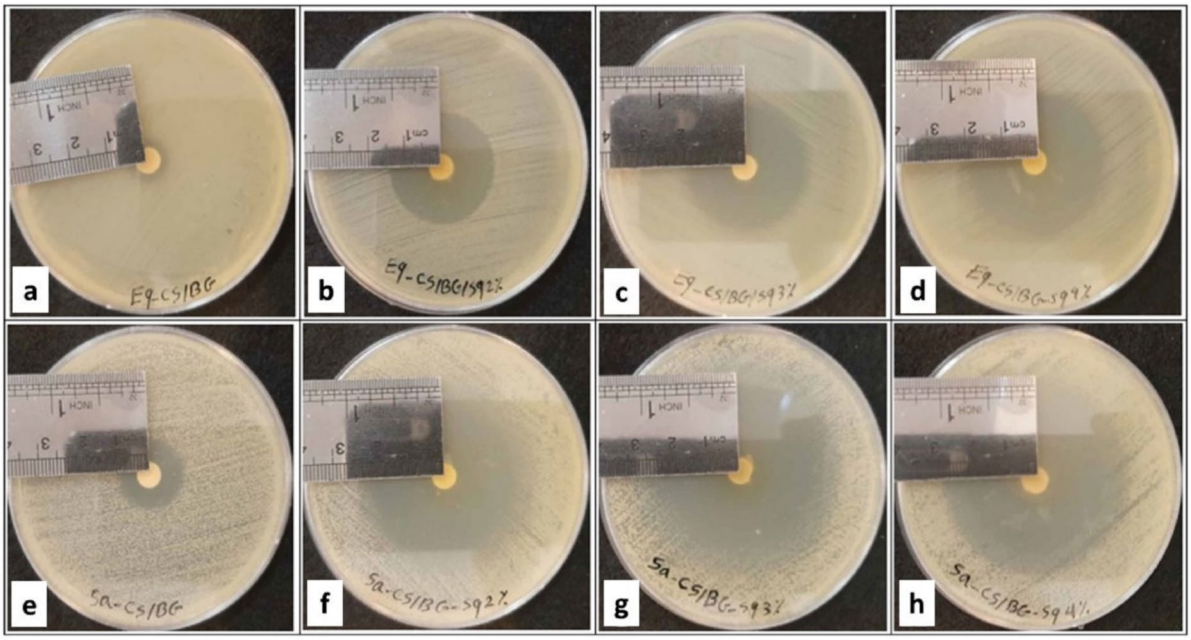

Fig. 10 The antibacterial effects of nanofibers and various concentrations of SQ. Free nanofibers exhibited negligible inhibitory zone against both bacterial strains (Fig. 8a and e). Cs/BG-SQ2% (Fig. 8b and f) had respectively 18 mm and 23 mm zone against *E. coli* and *S. aureus*. Cs/BG-SQ3% inferred 20 mm and 24 mm zone against *E. coli* and *S. aureus*, respectively. Additionally, Cs/BG-SQ4% deciphered 22 mm and 30 mm zone against *E. coli* and *S. aureus*, respectively

formulations containing PCL-PVA/Cs with a 2% concentration of SQ demonstrated exceptional anti-inflammatory properties, which are vital for effective wound healing. These advanced scaffolds not only promoted re-epithelialization but also improved the formation of granulation tissue and collagen deposition at the wound site. The sustained release of SQ directly at the wound location addresses the urgent need for effective local treatment strategies that reduce systemic side effects. Furthermore, by optimizing the SQ content in the scaffolds and creating a conducive healing environment through controlled drug release, these scaffolds represent a significant advancement in accelerating wound healing. Therefore, the approach utilized in this study holds promising potential for future developments in wound management.

Author Contributions Material preparation, data collection, and analysis were performed by Fariba Noori, Arash Goodarzi, Ali Abbasi, and Alireza Tavassoli. The first draft of the manuscript was written by Azam Bozorgi and other authors including Ahmad Reza Farmani, and Hassan Morovvati. Hiva Alipanah, Lida Ebrahimi, and Mohammad Reza Ataollahi reviewed the manuscript and commented on previous versions of the manuscript. Abdolmajid Ghasemian,collected the antibacterial data and analysed them and designed Figure 9. Fariba Noori, Ali Abbasi, Ahmad Reza Farmani and Azam Bozorgi prepared figures 1-5, and Table 2. Hassan Morovvati, Alireza Tavassoli, Mohammad Reza Ataollahi, Seyed Amin Kouhpayeh and Arash Goodarzi prepared Tables 1, 3, and 4 and Figures 6-8. Ahmad Reza Farmani, Azam Bozorgi, and other authors including Fariba Noori, and Arash Goodarzi revised the manuscript. All authors read and approved the final manuscript.

Funding This work was supported by School of Advanced Technologies in Medicine, Fasa University of Medical Sciences (Grant number 99038).

Data Availability No datasets were generated or analysed during the current study.

Declarations

Competing Interests The authors have no relevant financial or non-financial interests to disclose.

Ethical Approval This research has been conducted under ethical approval license IR.FUMS.AEC.1401.006.

Animal Studies Statement In vivo experiments were carried out according to the guidelines of the ethical committee of the Fasa University of Medical Sciences [Ethical code: IR.FUMS.AEC.1401.006].

References

1. Wei-MengWoo (2019) *Skin Structure and Biology*
2. Kukreja T, Saloki A, Saraf S (2024) A comprehensive review of a particular skin injury: pathogenesis, triggers, and current treatment options. Journal of Ravishankar University (PART-B)
3. Serra MB et al (2017) *From Inflammation to Current and Alternative Therapies Involved in Wound Healing.* International Journal of Inflammation, 2017
4. Landén NX, Li D, Ståhle M (2016) Transition from inflammation to proliferation: a critical step during wound healing. Cell Mol Life Sci 73(20):3861–3885

5. Mamun AA et al (2024) Recent advances in molecular mechanisms of skin wound healing and its treatments. Front Immunol 15:2024
6. Uberoi A, McCready-Vangi A, Grice EA (2024) The wound microbiota: microbial mechanisms of impaired wound healing and infection. Nat Rev Microbiol 22(8):507–521
7. Liang Y et al (2022) Antibacterial biomaterials for skin wound dressing. Asian J Pharm Sci 17:353–384
8. Azimi B et al (2020) Bio-based electrospun fibers for wound healing. J Funct Biomaterials 11(3):67
9. Liu X-k et al (2021) Electrospun Medicated Nanofibers Wound Healing: Rev Membr 11
10. Abrigo M, Mcarthur SL, Kingshott P (2014) Electrospun nanofibers as dressings for chronic wound care: advances, challenges, and future prospects. Macromol Biosci 14 6:772–792
11. Yang J, Xu L (2023) Electrospun nanofiber membranes with various structures for wound dressing. Mater (Basel), 16(17):6021
12. Zhang S et al (2024) Recent progress of electrospun nanofibers as burning dressings. RSC Adv 14(20):14374–14391
13. Wang Q et al (2024) Electrospun radially oriented berberine-PHBV nanofiber dressing patches for accelerating diabetic wound healing. Regen Biomater 11:1–14
14. Partovi A et al (2024) Electrospun nanofibrous wound dressings with enhanced efficiency through carbon quantum Dots and citrate incorporation. Sci Rep 14(1):19256
15. Zheng Q, Xi Y, Weng Y (2024) Functional electrospun nanofibers: fabrication, properties, and applications in wound-healing process. RSC Adv 14(5):3359–3378
16. Zhang X et al (2024) Advances in wound dressing based on electrospinning nanofibers. J Appl Polym Sci 141(1):e54746
17. Lu X, Zhou L, Song W (2024) Recent progress of electrospun nanofiber dressing in the promotion of wound healing. Polymers 16(18):2596
18. Li Y et al (2023) Advances, challenges, and prospects for surgical suture materials. Acta Biomater 168:78–112
19. Meng Q et al (2024) Recent advances of electrospun nanofiber-enhanced hydrogel composite scaffolds in tissue engineering. J Manuf Process 123:112–127
20. Alven S, Aderibigbe BA (2021) Fabrication of hybrid nanofibers from biopolymers and Poly (Vinyl Alcohol)/Poly (ε-Caprolactone) for Wound Dressing Applications. Polymers 13(13):2104
21. Xu R et al (2023) Recent advances in biodegradable and biocompatible synthetic polymers used in skin wound healing. Materials 16(15):5459
22. Iacob A-T et al (2020) An overview of biopolymeric electrospun nanofibers based on polysaccharides for wound healing management. Pharmaceutics 12(10):983
23. Buzgo M et al (2019) Poly-ε-Caprolactone and Polyvinyl alcohol electrospun wound dressings: adhesion properties and wound management of skin defects in rabbits. Regen Med 14(5):423–445
24. Mouro C, Simões M, Gouveia IC (2019) Emulsion electrospun Fiber Mats of PCL/PVA/Chitosan and Eugenol for wound dressing applications. Adv Polym Technol 2019(1):9859506
25. Abed EM et al (2025) Synthesis and evaluation of PCL/Chitosan/CQD-Fe magnetic nanocomposite for wound healing: emphasis on gene expression. Eng Life Sci 25(1):e202400038
26. Sperling LE et al (2016) Advantages and challenges offered by biofunctional core-shell fiber systems for tissue engineering and drug delivery. Drug Discovery Today 21 8:1243–1256
27. Abdullah MF et al (2019) Core-Shell fibers: design, roles, and controllable release strategies in tissue engineering and drug delivery. Polym (Basel) 11(12):1–45
28. Kazemi N et al (2024) Core-shell nanofibers containing L-arginine stimulates angiogenesis and full thickness dermal wound repair. Int J Pharm 653:123931
29. Criollo-Mendoza MS et al (2023) Wound healing properties of natural products: mechanisms of action. Molecules 28(2):1–18
30. Popa O et al (2015) *Methods for Obtaining and Determination of Squalene from Natural Sources.* BioMed Research International, 2015
31. Sánchez-Quesada C et al (2018) *Squalene Stimulates a Key Innate Immune Cell to Foster Wound Healing and Tissue Repair.* Evidence-based Complementary and Alternative Medicine: eCAM, 2018
32. Shanmugarajan TS, Selvan NK, Uppuluri V (2021) Development and characterization of Squalene-Loaded topical Agar-Based emulgel scaffold: wound healing potential in Full-Thickness burn model. Int J Low Extrem Wounds 20(4):364–373
33. Ma L et al (2019) Electrospun cellulose Acetate–Polycaprolactone/Chitosan Core–Shell nanofibers for the removal of Cr(VI). Phys Status Solidi (a) 216(22):1900379
34. Azari A et al (2022) Electrospun Polycaprolactone nanofibers: current research and applications in biomedical application. Adv Pharm Bull 12(4):658–672
35. Ghasemvand F et al (2023) Chitosan, polyethylene oxide/polycaprolactone electrospun core/shell nanofibrous mat containing Rosuvastatin as a novel drug delivery system for enhancing human mesenchymal stem cell osteogenesis. Front Mol Biosci 10:1220357
36. Musciacchio L et al (2025) Core-shell electrospun Polycaprolactone nanofibers, loaded with rifampicin and coated with silver nanoparticles, for tissue engineering applications. Biomaterials Adv 166:214036
37. Taokaew S, Chuenkaek T (2024) Developments of core/shell Chitosan-Based nanofibers by electrospinning techniques: A review. Fibers 12(3):26
38. Hadjianfar M et al (2021) *5FU-loaded PCL/Chitosan/Fe3O4 core-shell nanofibers structure: An approach to multi-mode anticancer system.* Advanced Pharmaceutical Bulletin, 12(3): p. 568
39. Ma L et al (2019) Electrospinning of Polycaprolacton/chitosan core-shell nanofibers by a stable emulsion system. Colloids Surf A 583:123956
40. Sivan M et al (2020) Plasma treatment effects on bulk properties of Polycaprolactone nanofibrous Mats fabricated by uncommon AC electrospinning: A comparative study. Surf Coat Technol 399:126203
41. Bulbul YE, Uygun A, Oksuz (2024) Cold atmospheric plasma modified Polycaprolactone solution prior to electrospinning: A novel approach for improving quercetin-loaded nanofiber drug delivery systems. Int J Pharm 651:123789
42. Yan D et al (2013) Plasma treatment of electrospun PCL random nanofiber meshes (NFMs) for biological property improvement. J Biomedical Mater Res Part A 101A(4):963–972
43. Fang Z et al (2023) Preparation and evaluation of Core–Shell nanofibers electrospun from PEU and PCL blends via a Single-Nozzle spinneret. ACS Appl Polym Mater 5(4):2382–2393
44. Tavakoli M et al (2024) Platelet rich fibrin and simvastatin-loaded pectin-based 3D printed-electrospun bilayer scaffold for skin tissue regeneration. Int J Biol Macromol 265:130954
45. Jahani M et al (2024) Antibacterial and wound healing stimulant nanofibrous dressing consisting of soluplus and soy protein isolate loaded with mupirocin. Sci Rep 14(1):26397
46. Mirhaj M et al (2024) A double-layer cellulose/pectin-soy protein isolate-pomegranate Peel extract micro/nanofiber dressing for acceleration of wound healing. Int J Biol Macromol 255:128198
47. Osanloo M et al (2024) The wound healing effect of polycaprolactone-chitosan scaffold coated with a gel containing Zataria multiflora Boiss. Volatile oil nanoemulsions. BMC Complement Med Ther 24(1):56

48. Osanloo M et al (2023) Effect of PCL nanofiber Mats coated with Chitosan microcapsules containing cinnamon essential oil for wound healing. BMC Complement Med Ther 23(1):84
49. Rahimi F et al (2023) Gelatin-based hydrogel functionalized with taurine moieties for in vivo skin tissue regeneration. Bio-Design Manuf 6(3):284–297
50. Akbari F et al (2022) Silico, in vitro, and in vivo wound healing activity of Astragalus microcephalus willd. Adv Pharmacol Pharm Sci 2022(1):2156629
51. Akbari F et al (2022) Vitro and in vivo wound healing activity of Astragalus floccosus Boiss. (Fabaceae). Adv Pharmacol Pharm Sci 2022(1):7865015
52. Gaikwad S et al (2022) Superior in vivo wound-Healing activity of mycosynthesized silver nanogel on different wound models in rat. Front Microbiol 13
53. Dehghani S et al (2020) Topical application of Curcumin regulates the angiogenesis in diabetic-impaired cutaneous wound. Cell Biochem Funct 38(5):558–566
54. Veličković V, Janković D (2023) Challenges around quantifying uncertainty in a holistic approach to hard-to-heal wound management: health economic perspective. Int Wound J 20(3):792–798
55. Ebrahimi L et al (2021) Metformin-Loaded PCL/PVA fibrous scaffold preseeded with human endometrial stem cells for effective guided bone regeneration membranes. ACS Biomaterials Sci Eng 7(1):222–231
56. Godoi MM et al (2024) Perspective from developers: Tissue-engineered products for skin wound healing. Int J Pharm Volume 660:124319
57. Salehi M et al (2020) Electrospun Poly (ε-caprolactone)/gelatin nanofibrous mat containing selenium as a potential wound dressing material: in vitro and in vivo study. Fibers Polym 21:1713–1721
58. Palani N et al (2024) Electrospun nanofibers synthesized from polymers incorporated with bioactive compounds for wound healing. J Nanobiotechnol 22(1):211
59. Fu W et al (2024) Opportunities and challenges of nanomaterials in wound healing: advances, mechanisms, and perspectives. Chem Eng J 495:153640
60. Whittam AJ et al (2016) Challenges and opportunities in drug delivery for wound healing. Adv Wound Care 5(2):79–88
61. Miguel SP et al (2019) An overview of electrospun membranes loaded with bioactive molecules for improving the wound healing process. Eur J Pharm Biopharm 139:1–22
62. Shanmugarajan T, Selvan NK, Uppuluri VNVA (2021) Development and characterization of squalene-loaded topical agar-based emulgel scaffold: wound healing potential in full-thickness burn model. Int J Low Extrem Wounds 20(4):364–373
63. Movahedi M et al (2019) Potential of novel electrospun core-shell structured polyurethane/starch (hyaluronic acid) nanofibers for skin tissue engineering: in vitro and in vivo evaluation. International journal of biological macromolecules
64. Makita H, Hastings G (2018) *Time-resolved step-scan FTIR difference spectroscopy for the study of photosystem I with different benzoquinones incorporated into the A1 binding site.* Biochimica et biophysica acta. Bioenergetics 1859 11:1199–1206
65. Barzegar S et al (2021) Core-shell chitosan/PVA-based nanofibrous scaffolds loaded with Satureja mutica or Oliveria decumbens essential oils as enhanced antimicrobial wound dressing. Int J Pharm 597:120288
66. Lee NM et al (2017) Polymer fiber-based models of connective tissue repair and healing. Biomaterials 112:303–312
67. Mouro C, Gomes AP, Gouveia IC (2023) Emulsion electrospinning of PLLA/PVA/Chitosan with Hypericum perforatum L. as an antibacterial nanofibrous wound dressing. Gels 9(5):353
68. Camera E, Ottaviani M, Picardo M (2015) *Squalene Chemistry and Biology*, in *Lipids and Skin Health*, A. Pappas, Editor. Springer International Publishing: Cham. pp. 185–198
69. Medina A, Pineda A, Treviño C (2003) Imbibition driven by a temperature gradient. J Phys Soc Jpn 72(5):979–982
70. Ivanova S et al (2015) Surface properties of squalene/Meibum films and NMR confirmation of squalene in tears. Int J Mol Sci 16(9):21813–21831
71. Huang Z-R, Lin Y-K, Fang J-Y (2009) Biological and Pharmacological activities of squalene and related compounds: potential uses in cosmetic dermatology. Molecules 14(1):540–554
72. Shalu S et al (2024) Microbial squalene: A sustainable alternative for the cosmetics and pharmaceutical Industry– A review. Eng Life Sci 24(10):e202400003
73. Fox CB (2009) Squalene emulsions for parenteral vaccine and drug delivery. Molecules 14(9):3286–3312
74. Zheng J-Y et al (2014) The effect of surfactants on the diameter and morphology of electrospun ultrafine nanofiber. J Nanomaterials 2014(1):689298
75. Abutaleb A et al (2017) Effects of surfactants on the morphology and properties of electrospun polyetherimide fibers. Fibers 5(3):33
76. Johnson PM et al (2021) Surfactant location and internal phase volume fraction dictate emulsion electrospun fiber morphology and modulate drug release and cell response. Biomater Sci 9(4):1397–1408
77. Fang W et al (2017) Effects of various surfactants on alkali lignin electrospinning ability and spun fibers. Ind Eng Chem Res 56(34):9551–9559
78. Jia L, Qin X (2013) The effect of different surfactants on the electrospinning poly(vinyl alcohol) (PVA) nanofibers. J Therm Anal Calorim 112:595–605
79. Tarasova EV et al (2015) Formation of uniform PVDF fibers under ultrasound exposure in presence of anionic surfactant. J Electrostat 76:39–47
80. Zhao J et al (2016) Effect of surface-active agent on morphology and properties of electrospun PVA nanofibres. Fibers Polym 17:896–901
81. Talib Al-Sudani B et al (2024) Vasculo-osteogenic keratin-based nanofibers containing merwinite nanoparticles and sildenafil for bone tissue regeneration. Int J Pharm 667:124875
82. Aydın S et al (2022) A comparison study of Fiber diameter effect on characteristic features of Donepezil/Curcumin-Loaded Polycaprolactone/Polylactic acid nanofibers. Macromolecular Materials and Engineering
83. Yousefi I et al (2017) An investigation of electrospun Henna leaves extract-loaded Chitosan based nanofibrous Mats for skin tissue engineering. Mater Sci Engineering: C 75:433–444
84. Zhang H, Zhou L, Zhang W (2014) Control of scaffold degradation in tissue engineering: a review. Tissue Eng Part B Rev 20(5):492–502
85. Echeverria Molina MI, Malollari KG, Komvopoulos K (2021) Design challenges in polymeric scaffolds for tissue engineering. Front Bioeng Biotechnol 9:617141
86. Costa MA et al (2018) Biophysical characterization of asolectin-squalene liposomes. Colloids Surf B 170:479–487
87. Roy T et al (2018) Core-Shell nanofibrous scaffold based on Polycaprolactone-Silk fibroin emulsion electrospinning for tissue engineering applications. Bioengineering 5(3):68
88. Suamte L et al (2023) Various manufacturing methods and ideal properties of scaffolds for tissue engineering applications. Smart Mater Manuf 1:100011
89. Selestin Raja I et al (2022) Predominant factor influencing cellular behaviors on electrospun nanofibrous scaffolds: wettability or surface morphology? Materials & Design

90. Oliveira SM, Alves NM, Mano JF (2014) Cell interactions with superhydrophilic and superhydrophobic surfaces. J Adhes Sci Technol 28(8–9):843–863
91. Singh R et al (2018) Fabrication and characterization of Core-Shell nanofibers using a Next-Generation airbrush for biomedical applications, vol 10 49. ACS applied materials & interfaces, pp 41924–41934
92. Jiang C et al (2021) Textile-based sandwich scaffold using wet electrospun yarns for skin tissue engineering. J Mech Behav Biomed Mater 119:104499
93. Zahedi E et al (2019) Fabrication and characterization of Core-Shell electrospun fibrous Mats containing medicinal herbs for wound healing and skin tissue engineering. Mar Drugs 17(1):27
94. Gavande V, Nagappan S, Lee W-K (2022) Considering electrospun nanofibers as a filler network in electrospun Nanofiber-Reinforced composites to predict the tensile strength and Young's Modulus of nanocomposites: A modeling study. Polymers 14(24):5425
95. Warleta F et al (2010) Squalene protects against oxidative DNA damage in MCF10A human mammary epithelial cells but not in MCF7 and MDA-MB-231 human breast cancer cells. Food Chem Toxicology: Int J Published Br Industrial Biol Res Association 48(4):1092–1100
96. Kornienko J et al (2019) High doses of synthetic antioxidants induce premature senescence in cultivated mesenchymal stem cells. Sci Rep 9
97. Chen W et al (2014) High concentrations of genistein exhibit pro-oxidant effects in primary muscle cells through mechanisms involving 5-lipoxygenase-mediated production of reactive oxygen species. Food Chem Toxicology: Int J Published Br Industrial Biol Res Association 67:72–79
98. Oishi Y, Manabe I (2018) Macrophages in inflammation, repair and regeneration. Int Immunol 30(11):511–528
99. Mirhaj M et al (2023) Mupirocin loaded core-shell pluronic-pectin-keratin nanofibers improve human keratinocytes behavior, angiogenic activity and wound healing. Int J Biol Macromol 253:126700
100. Pajooh AMD et al (2024) Biomimetic VEGF-loaded bilayer scaffold fabricated by 3D printing and electrospinning techniques for skin regeneration. Mater Design 238:112714
101. Micera M et al (2020) Squalene: more than a step toward sterols. Antioxidants 9(8):688
102. Tavakoli M et al (2023) Keratin- and VEGF-Incorporated Honey-Based Sponge–Nanofiber dressing: an ideal construct for wound healing. ACS Appl Mater Interfaces 15(48):55276–55286
103. Mirhaj M et al (2023) An antibacterial Multi-Layered scaffold fabricated by 3D printing and electrospinning methodologies for skin tissue regeneration. Int J Pharm 645:123357
104. Ulrikh EV, Smolovskaya OV (2022) Evaluation of anti-inflammatory and wound healing properties of squalene: an important phytochemical component of Amaranth oil. IJCBS 21:54–60
105. Kaseke T, Opara UL, Fawole OA (2020) Fatty acid composition, bioactive phytochemicals, antioxidant properties and oxidative stability of edible fruit seed oil: effect of preharvest and processing factors. Heliyon 6(9):e04962
106. Chen S et al (2017) Recent advances in electrospun nanofibers for wound healing. Nanomed (Lond) 12(11):1335–1352
107. Gill AS et al (2023) Synthetic polymer based electrospun scaffolds for wound healing applications. J Drug Deliv Sci Technol 89:105054
108. Su C et al (2022) Functionalized electrospun Double-Layer nanofibrous scaffold for wound healing and Scar Inhibition. ACS Omega 7(34):30137–30148
109. Afsharian YP, Rahimnejad M (2021) Bioactive electrospun scaffolds for wound healing applications: A comprehensive review. Polym Test 93:106952
110. Flores-Rojas GG et al (2023) Electrospun scaffolds for tissue engineering: A review. Macromol 3(3):524–553
111. Khorshidi S et al (2016) A review of key challenges of electrospun scaffolds for tissue-engineering applications. J Tissue Eng Regen Med 10(9):715–738
112. Dang Z et al (2024) Electrospun nanofiber scaffolds loaded with Metal-Based nanoparticles for wound healing. Polymers 16(1):24
113. Dodero A et al (2020) Investigation of the mechanical and Dynamic-Mechanical properties of electrospun Polyvinylpyrrolidone membranes: A design of experiment approach. Polym (Basel) 12(7):1–17
114. Shamirzaei Jeshvaghani E et al (2018) Fabrication, characterization, and biocompatibility assessment of a novel elastomeric nanofibrous scaffold: A potential scaffold for soft tissue engineering. J Biomedical Mater Res Part B: Appl Biomaterials 106(6):2371–2383
115. Yadav PD et al (2024) Electrospun composite nanofibers for wound healing: synthesis, characterization, and clinical potential of biopolymer-based materials. Discover Mater 4(1):99
116. Suamte L, Babu PJ (2024) Electrospun based functional scaffolds for biomedical engineering: A review. Nano TransMed 3:100055

Terms and Conditions

Springer Nature journal content, brought to you courtesy of Springer Nature Customer Service Center GmbH (“Springer Nature”).
Springer Nature supports a reasonable amount of sharing of research papers by authors, subscribers and authorised users (“Users”), for small-scale personal, non-commercial use provided that all copyright, trade and service marks and other proprietary notices are maintained. By accessing, sharing, receiving or otherwise using the Springer Nature journal content you agree to these terms of use (“Terms”). For these purposes, Springer Nature considers academic use (by researchers and students) to be non-commercial.
These Terms are supplementary and will apply in addition to any applicable website terms and conditions, a relevant site licence or a personal subscription. These Terms will prevail over any conflict or ambiguity with regards to the relevant terms, a site licence or a personal subscription (to the extent of the conflict or ambiguity only). For Creative Commons-licensed articles, the terms of the Creative Commons license used will apply.
We collect and use personal data to provide access to the Springer Nature journal content. We may also use these personal data internally within ResearchGate and Springer Nature and as agreed share it, in an anonymised way, for purposes of tracking, analysis and reporting. We will not otherwise disclose your personal data outside the ResearchGate or the Springer Nature group of companies unless we have your permission as detailed in the Privacy Policy.
While Users may use the Springer Nature journal content for small scale, personal non-commercial use, it is important to note that Users may not:

1. use such content for the purpose of providing other users with access on a regular or large scale basis or as a means to circumvent access control;
2. use such content where to do so would be considered a criminal or statutory offence in any jurisdiction, or gives rise to civil liability, or is otherwise unlawful;
3. falsely or misleadingly imply or suggest endorsement, approval , sponsorship, or association unless explicitly agreed to by Springer Nature in writing;
4. use bots or other automated methods to access the content or redirect messages
5. override any security feature or exclusionary protocol; or
6. share the content in order to create substitute for Springer Nature products or services or a systematic database of Springer Nature journal content.

In line with the restriction against commercial use, Springer Nature does not permit the creation of a product or service that creates revenue, royalties, rent or income from our content or its inclusion as part of a paid for service or for other commercial gain. Springer Nature journal content cannot be used for inter-library loans and librarians may not upload Springer Nature journal content on a large scale into their, or any other, institutional repository.
These terms of use are reviewed regularly and may be amended at any time. Springer Nature is not obligated to publish any information or content on this website and may remove it or features or functionality at our sole discretion, at any time with or without notice. Springer Nature may revoke this licence to you at any time and remove access to any copies of the Springer Nature journal content which have been saved.
To the fullest extent permitted by law, Springer Nature makes no warranties, representations or guarantees to Users, either express or implied with respect to the Springer nature journal content and all parties disclaim and waive any implied warranties or warranties imposed by law, including merchantability or fitness for any particular purpose.
Please note that these rights do not automatically extend to content, data or other material published by Springer Nature that may be licensed from third parties.
If you would like to use or distribute our Springer Nature journal content to a wider audience or on a regular basis or in any other manner not expressly permitted by these Terms, please contact Springer Nature at

onlineservice@springernature.com